

Publication status: Preprint has not been submitted for publication

# Kalman Filters in crop models: old experiences in new contexts

Monique Pires Gravina de Oliveira, Thais Queiroz Zorzeto-Cesar, Romis Ribeiro de Faissol Attux,  
Luiz Henrique Antunes Rodrigues

<https://doi.org/10.1590/SciELOPreprints.8033>

Submitted on: 2024-02-04

Posted on: 2024-02-06 (version 1)

(YYYY-MM-DD)

1 **Preprint** of manuscript *Kalman Filters in crop models: old experiences in new contexts* This

2 version of the manuscript has not been peer-reviewed.

3 2024-02-03

4

## 5 **Kalman Filters in crop models: old experiences in new contexts**

6 **Monique Pires Gravina de Oliveira<sup>a1\*</sup>, Thais Queiroz Zorzeto-Cesar<sup>a2</sup>, Romis Ribeiro de**  
7 **Faissol Attux<sup>b3</sup>, Luiz Henrique Antunes Rodrigues<sup>a4</sup>**

8 <sup>a</sup> Universidade Estadual de Campinas (UNICAMP), Faculdade de Engenharia Agrícola  
9 Av. Cândido Rondon, 501 - Cidade Universitária - 13083-875 - Campinas, SP, Brazil

10 <sup>b</sup> Universidade Estadual de Campinas (UNICAMP), Faculdade de Engenharia Elétrica e de  
11 Computação, Departamento de Engenharia de Computação e Automação Industrial.  
12 Av. Albert Einstein, 400 - Cidade Universitária -13083-970 - Campinas, SP, Brazil

13 <sup>1</sup> [moniquepgoliveira@gmail.com](mailto:moniquepgoliveira@gmail.com) , <https://orcid.org/0000-0001-7167-4473>

14 <sup>2</sup> [thaisqzc@unicamp.br](mailto:thaisqzc@unicamp.br) , <https://orcid.org/0000-0001-6959-7990>

15 <sup>3</sup> [attux@unicamp.br](mailto:attux@unicamp.br) , <https://orcid.org/0000-0002-2961-4044>

16 <sup>4</sup> [lique@unicamp.br](mailto:lique@unicamp.br) , <https://orcid.org/0000-0002-1756-7367>

17 \* Corresponding author

18

### 19 **ABSTRACT**

20 Data assimilation has been widely used for improvement of crop models' estimates, for  
21 example to incorporate the effects of external events or compensate calibration errors in large  
22 areas. The term describes multiple approaches for those who want to take advantage of satellite  
23 imagery to reduce uncertainty or improve accuracy of model estimates. Kalman Filters are  
24 among the most used methods for achieving these goals. But their use in new contexts, i.e.,  
25 from open field to protected environments, requires untangling aspects of the pipeline that are  
26 often performed in many different ways without guidelines, such as which variables to  
27 assimilate or how to ascribe uncertainty to observations or model estimates. This study is then  
28 divided in two parts. In the first, we review details on how uncertainty is ascribed on crop model  
29 estimates and in observations for applications of the Kalman Filter and three variations of the

30 method, i.e., the Extended, Unscented and Ensemble, as well as which state variables are often  
31 updated and the frequency with which assimilation may occur, as well as how these aspects are  
32 connected to each other. In the second part, we apply different approaches from the reviewed  
33 literature in a greenhouse tomato crop model. We use artificial data with controlled noise levels  
34 as well as artificial data generated by simulation using other tomato crop model. We assess the  
35 impacts of using different methods and different approaches for ascribing uncertainty in model  
36 estimates and in observations, by assimilating artificial observations of fruit and of mature fruit  
37 biomass. We note that covariances should not be fixed values, that there are trade-offs between  
38 ascribing model uncertainty to the state itself and to other elements of the process, that  
39 observation covariance may have been considered disproportionality higher when using some  
40 ensemble generation approaches in the EnKF, and that bias in model estimates may lead to  
41 worse outcomes even when observations are high-quality ones. While we discussed aspects that  
42 should be considered in a new environment, many of them are also important for field crops,  
43 and we concluded assimilation should follow an assessment of which variables could be useful  
44 for assimilation.

45

46 Keywords: crop model; data assimilation; protected environments; uncertainty; state estimation

47

## 48 **1 INTRODUCTION**

49 Data assimilation on crop models has mostly been performed by the integration of remote  
50 sensing Earth observations into process-based crop models, often with the goal of improving  
51 agricultural systems' models predictive capability. Technical aspects of the discipline have  
52 frequently been revisited given the evolution in computational capacity and available state  
53 estimation techniques [1–5]. These reviews, which detail how the approach has been used in  
54 crop modelling, have looked into the subject from different perspectives, such as the methods

55 used to derive biophysical and biochemical canopy state variables from optical remote sensing  
56 data in the VNIR-SWIR regions [2], the sources of errors in each element of the data  
57 assimilation process [3], the theoretical basis for methods as well as a walkthrough of the steps  
58 required to apply them [4], and the models and quantities being assimilated [5]. These studies,  
59 however, emphasize limitations and aspects related to satellite-derived observations, e.g. the  
60 spatial and temporal scale of satellite images [3–5].

61 In this sense, many of the lessons that have been learned by the crop modelling and remote  
62 sensing community could still be discussed and extended into other agricultural domains.  
63 Protected environments, for instance, allow for more intense monitoring, e.g. with daily pictures  
64 [6,7], without the adverse effects of large scale. It could be useful to explore assimilation  
65 techniques to enhance accuracy and reduce uncertainty in model estimates obtained in the  
66 context of these environments. In the steps suggested by Huang et al. (2019) [4], assimilating  
67 observations requires some pre-data assimilation considerations concerning the model and the  
68 observations, characterizing uncertainties, and solving a scale mismatch problem between  
69 observations and models. In the proposed new context, the first two would be the more relevant  
70 steps.

71 Luo et al (2023) [5] quantified which state variables and models are the more frequently  
72 explored in data assimilation studies with remote sensing data and, for variables, leaf area index  
73 was unquestionably the most used. They give multiple reasons, but one relevant aspect not  
74 mentioned is the previous existence of products that allow for coupling model estimates and  
75 outputs of satellite images. For different crops and data sources, these are relationships that  
76 must be established. And they should be defined to represent the variables that could in fact be  
77 useful for assimilation, since not always updating one variable would lead to improvement in  
78 another [8,9]. Furthermore, the models they mentioned as most used would likely not be used  
79 in protected environments, for horticultural or ornamental crops. Therefore, the uncertainty

80 quantification step would be required for them, as well as for these new relationships and  
81 observations. Additionally, while the remote sensing realm is dependent on revisit frequency  
82 and is vulnerable to unfavorable atmospheric conditions, leading to fewer observations  
83 available, the high-frequency potentially noisy observations of a greenhouse environment  
84 [10,11] could become a hindrance.

85 To better understand how these differences could impact new studies, it is useful to  
86 explore artificial data, so that it is possible to investigate the behavior of the system with more  
87 methodological control. These types of studies have sometimes been called Observation System  
88 Synthetic Experiments (OSSE) [9,12] or synthetic twin [13] and have been used for answering  
89 questions such as if the assimilation of an observation improves all components of the model's  
90 simulations, if calibration errors can be compensated by assimilation [12], which are limitations  
91 imposed by the model, the assimilation method, and uncertainty in model inputs and  
92 observations [9], appropriate ensemble size [13], and to test new methods [14].

93 This study is then divided in two parts. In the first part, we revisit applications of data  
94 assimilation in crop models, describing the general use of Kalman Filters and focusing on the  
95 steps of uncertainty characterization. In the following sections, we assess how they relate to  
96 performance and use as example a greenhouse tomato growth model — the Reduced-State  
97 Tomgro model [15] —aiming at improving yield estimates through assimilating artificial  
98 observations of tomatoes in a greenhouse environment.

## 99 **2 BACKGROUND**

100 The reviews of data assimilation in crop models previously mentioned [1–5] categorize  
101 three types of data assimilation: forcing, calibration and update. Given the broad scope of three  
102 approaches and the several methods that exist to explore them, this study will only comment on  
103 the update approach using filters from the Kalman Family, which are very frequently used [5],  
104 focusing on the elements more connected to the uncertainty characterization. The reviews also

105 explain the methods in detail, so we refer to them, especially Huang et al. (2019) [4], for the  
106 mathematical equations of the filters.

## 107 **2.1 Crop models**

108 Briefly, crop models are mathematical representations of plants throughout their growth  
109 as affected by the factors that influence said growth, e. g. crop's genetics and the environment.  
110 De Vries (1982) proposed three levels of complexity for categorizing crop models: preliminary,  
111 comprehensive, or summary models. While the first type contains basic features of the system  
112 and aims at a first understanding of the subject, once more knowledge into the processes is  
113 gained and imbued into the model, it becomes closer to the second type which, to be made more  
114 accessible to others, may then be simplified into the third type, depending on the intended use  
115 of the model. Passioura (1996) discussed two other categories, which are related to the intent  
116 of their development and use: they could be aimed at farmers, to aid in their decision-making  
117 and, for that, understanding of the underlying mechanisms would not be required, or they could  
118 be aimed at scientific purposes, which means that the description of mechanisms should be  
119 related to theories and validated by hypothesis testing. The first case is generally associated  
120 with the terms functional, empirical, statistical and phenomenological and the second, to the  
121 terms mechanistic and process-based [18]. In this study, we explore process-based crop models,  
122 given their ability to represent interactions between state variables.

## 123 **2.2 Kalman Filter methods and their requirements**

### 124 **2.2.1 The Kalman Filter (KF)**

125 The main assumptions of the Kalman Filter are that the model estimates and the  
126 observations follow a normal distribution, and that the process model and the observation  
127 function are linear, but if the non-linear crop model can be assumed locally linear between  
128 adjacent time steps, the standard Kalman Filter could be a viable choice [4].

129           Given its restrictions, there are fewer examples of the application of this technique. In  
130 some of them, the premise of the filter is used, but with modifications. Instead of calculating  
131 the gain, Vazifedoust et al. (2009) [19] tested different values, using the best one as fixed,  
132 circumventing the need for identifying the source error values. This approach was repeated by  
133 Chen, Zhang and Tao (2018) [20], who also normalized simulated and observation values  
134 according to the maximum value obtained so that they would be in the same range. Operating  
135 in this normalized space allowed them to focus on spatial variability and, in part, trends, instead  
136 of absolute values. Later, Chen and Tao (2020) [21] explored more approaches for defining an  
137 appropriate value for the fixed gain, by a grid search of an optimal value, as well as exploring  
138 historical values.

### 139 **2.2.2 Extended Kalman Filter (EKF)**

140           The Extended Kalman Filter is an adaptation of the Kalman Filter to deal with non-linear  
141 cases. To do so, it takes advantage of local linearization by replacing the model and the  
142 measurement function by their partial derivatives. The use of this technique is also limited, as  
143 it requires access to the Jacobian of the model or, in some cases, to an approximation by finite  
144 differences that often will not scale to higher dimensions [4], so there are also few examples on  
145 crop modeling that apply this technique.

146           One of these few examples in which there is an explanation of how the filter was used is  
147 the study of Linker and Ioslovich (2017) [22]. The authors used data from growth experiments  
148 of cotton and potatoes aiming at improving estimates of canopy cover and biomass through  
149 state assimilation and through the recalibration of three parameters from the Aquacrop model.  
150 Given there were two different approaches for improving estimates, they estimated the  
151 covariance matrix of the errors in the state variables in two ways. For the assimilation process,  
152 by calculating the difference between the square of the model residuals and the dispersion of  
153 the measurements. They chose not to propagate the matrix along the process, given its strong

154 nonlinearity, and recalculated it at each new time of measurement. They justified this choice by  
155 claiming the propagation without assimilation of new measurements would only increase the  
156 uncertainty related to the linearization and to the unknown initial data of the model errors. For  
157 the recalibration process, the matrix was calculated using an assumption that the corresponding  
158 standard deviation of each of the chosen parameters is equal to 20% of the current value of  
159 corresponding parameter. In their assimilation approach, the H matrix, i.e., that used for the  
160 linearization, corresponded to the unit matrix, as the measurements directly corresponded to the  
161 states and, in the recalibration one, the components of the partial derivatives matrix H were  
162 calculated numerically at each instance of canopy cover measurement.

### 163 **2.2.3 Ensemble Kalman Filter (EnKF)**

164 Overall, in the Ensemble Kalman Filter, an ensemble of initial states is generated and  
165 each individual ensemble member is propagated through the model until an observation is  
166 available. Then the update step is performed individually in each member. This allows for  
167 recalculation of the ensemble mean for the states and generation of a new ensemble. The  
168 ensemble approach operates on the underlying assumption that at least some of the particles  
169 will represent the true state [12]. There are, however, different ways of approaching this  
170 problem and the elements of uncertainty are intimately connected to other decisions.

#### 171 *Composition of ensemble elements*

172 The uncertainty associated with the model derives from the variability in the ensemble.  
173 Therefore, the choice of how to generate these elements is reflected on how much the filter will  
174 rely on the models' estimates. There have been many approaches for doing so, dealing with  
175 every element involved in the simulations, i.e., inputs, parameters, or states.

176 Input perturbation examples come from Lei et al. (2020) [13], who perturbed precipitation  
177 and irrigation inputs via multiplicative rescaling with mean-unity lognormally distributed  
178 random errors that have a standard deviation equal to 20% of the corresponding input, and from

179 De Wit and Van Diepen (2007) [23], who generated precipitation ensembles based on a highly  
180 accurate precipitation dataset that was perturbed with an additive error component and a  
181 multiplicative component that generated binary rain or no-rain events on locations in which the  
182 records pointed to the absence of precipitation. In Oliveira et al. (2023) [24], the authors  
183 explored the uncertainty existent in measurements of low-cost luxmeters to perturb the  
184 photosynthetically active radiation measurements used as inputs in the model.

185 In cases in which states are perturbed, Xie et al. (2017) [25] input the initial states and  
186 parameters into the CERES-Wheat and, at the beginning of the green-up stage, LAI and soil  
187 moisture were perturbed according to the errors between the field measurements and the  
188 simulated LAI and soil moisture. Ines et al. (2013) [26] randomly sampled, at the start of the  
189 simulation, values of leaf weight at emergence and plant leaf area at emergence, to increase the  
190 variability of the ensemble. Beyond inputs, Lei et al. (2020) [13] also applied direct  
191 perturbations to soil moisture states at all depths independently with random errors sampled  
192 from a mean-zero, normal distribution with temporally varying standard deviation equal to 10%  
193 of the state value, followed by the introduction of a vertical auto-correlation at the different  
194 depths. Kang and Özdoğan (2019) [8] not only perturbed the initial aboveground biomass or  
195 LAI for each ensemble member to simulate model noise, but also initial soil water content, to  
196 simulate variations in soil properties and water balance.

197 Researchers have used multiple ways of ascribing uncertainty to parameters. Kang and  
198 Özdoğan (2019) [8] added random noises drawn from a uniform distribution ranges from 0 to  
199 10% of the original values of soil hydraulic parameter. They also chose a parameter that should  
200 vary over the course of the growing season and that accounts for stress not simulated by the  
201 model to perturb with noise sampled from a uniform distribution centered in the original value.  
202 Huang et al. (2016) [27] chose the parameters based on the results of a sensitivity analysis and  
203 set the values of the standard deviations of two parameters, following the results of a previous

204 study. Ines et al. (2013) [26] identified which parameters had major influence in the model and,  
205 with an uncertainty level of 10%, perturbed each model parameter using a Gaussian  
206 distribution, generating ensemble members by randomly sampling model parameter  
207 combinations from the perturbed arrays. Zhao, Chen and Shen (2013) [28] even tried to evaluate  
208 the impact of using parameter uncertainty to generate the ensembles. They chose one parameter  
209 that was mostly correlated to crop yield and ascribed a distribution to it, multiplying its standard  
210 deviation by different fixed values. Lu et al. (2021) [29] took advantage of the existing  
211 uncertainty in parameters and used this as an artifact to generate ensembles without calibrating  
212 the model. They sampled parameters that they called variant as well as a fixed factor to scale  
213 phenological parameters for the canopy in a given year.

214 One issue in perturbing parameters or inputs for generating the ensembles is what Curnel  
215 et al. (2011) [30] denominated phenological shift. This effect refers to ensemble elements that  
216 are in different phenological stages, which leads, at the same point in the simulation, to different  
217 modules in the model to be active and, therefore, the assimilation of an observation having  
218 different a meaning for each ensemble member.

219 As for the perturbation used in observations — which are also treated as random variables  
220 to add to the variance of the updated ensemble [31] — Ines et al. (2013) [26] state that the  
221 variance used in its generation is based on the uncertainty of the data. But more precisely,  
222 Huang et al. (2016) [27] mentions that the standard deviation of the Gaussian white noise error  
223 needs to be a realistic value for it to represent the uncertainty of the remotely sensed  
224 observation. In section 2.3, uncertainties in observations are more thoroughly described, but as  
225 an example, Xie et al. (2017) [25] used the differences between field measurements and remote  
226 sensing observations to determine the standard deviations of the observed LAI and soil  
227 moisture.

228            *Ensemble size*

229            The choice of ensemble size is often performed in three different ways: testing,  
230            referencing a theoretical result or referencing other assimilation study on the literature. Pellenq  
231            and Boulet (2004) [12] affirmed a preliminary study must be performed to find the minimum  
232            ensemble size that ensures particles may follow the same trajectory as the true state. They say  
233            the number usually corresponds to value above which assimilation results are identical. With  
234            this approach, Nearing et al. (2012) [9] showed an example in which the number depended on  
235            the goal of the assimilation. The authors tested different values when assimilating LAI and soil  
236            moisture aiming at improving estimates of wheat yield, LAI and soil moisture. In the cases of  
237            assimilation of the state variable, RMSE became stable with number of elements of 25. In the  
238            other cases, the stability came with an ensemble of 100 elements. Lu et al. (2021) [29] evaluated  
239            ensemble sizes for simultaneous assimilation of canopy cover and soil moisture from 10 to 400  
240            and overall observed little improvement for more than 200, even though in some years 10  
241            elements were enough for stable results.

242            Several studies, however, refer to the experiences of other authors. Frequently, authors  
243            refer to De Wit and Van Diepen (2007) [23] when commenting on their choice for the ensemble  
244            size [28,32,33] The study, however, applies to assimilating soil moisture with an ensemble  
245            obtained by perturbing precipitation and with an initial state ascribed by sampling a calculated  
246            Gaussian acceptable value and it is possible that they do not generalize for other approaches.  
247            Additionally, the authors mention that although they observed reduced RMSE in soil moisture  
248            estimates, this was not applied to the variance. Despite that, their results were compatible with  
249            other results for soil moisture, and Mishra, Cruise and Mecikalski (2021) [34] followed the  
250            suggestion from the study of Yin et al. (2015) [35], who theoretically and through an example  
251            showed that the ideal ensemble size for assimilating soil moisture is 12, which suggests 50  
252            would be a reasonable estimate in similar situations.

#### 253 **2.2.4 Unscented Kalman Filter (UKF)**

254         Similarly to the EnKF, the Unscented Kalman Filter uses the average of an ensemble as  
255 the state estimate, instead of the direct estimates provided by the model. However, the ensemble  
256 is not just sampled from a distribution. It uses what is called the unscented transform to generate  
257 particles — the sigma points — and weights for those particles that, when combined, are more  
258 representative of the expected state value. These sigma points are propagated through the non-  
259 linear model, which provides more accurate approximations of the mean and covariance matrix  
260 of the state vector, and thus more accurate state estimation. [36].

261         Torres-Monsivais et al. (2017) [37] evaluated the UKF along with data simulated with  
262 the Reduced State Tomgro model, perturbed by several noise levels. Ruíz-García et al. (2014)  
263 [38] used data from destructive analyses of lettuce in a greenhouse to assess uncertainty of the  
264 NICOLET model. In the study with tomato, the authors ascribed low covariances to the model  
265 and higher to the measurements, and assessed the UKF performance given noise added to model  
266 estimates, while in the study with lettuce, the values were tuned until reasonable results were  
267 obtained. Recently, Belozerova (2023) [39] emphasized the UKF advantages over the EnKF,  
268 namely, its non-stochastic behavior and its being computationally cheaper, with comparable  
269 performance.

#### 270 **2.3 Errors and uncertainty**

271         How to identify errors in the elements involved in assimilation and quantify their  
272 uncertainties is widely discussed by Jin et al. (2018) [3] and Huang et al. (2019a) [4], as they  
273 are central in filtering approaches. For crop models, the sources of uncertainty they list include  
274 not only issues referring to how processes are represented and the quality of input data, but also  
275 the difference between simulations and actual growth, which is impacted by pests and diseases.  
276 For observations, they mention errors in the measurement themselves and in retrieval methods.  
277 In both cases, often their studies emphasize aspects of satellite-derived observations, such as

278 errors in spatial data and scale mismatches. This section aims to revisit this topic, with more  
279 details and examples on how these uncertainties have been quantified and applied in data  
280 assimilation studies. Although the discussion in this section focus on trying to ascribe meaning  
281 and understanding the uncertainties, these are filter hyperparameters that may be estimated from  
282 data [40].

### 283 **2.3.1 Observations**

284 Overall, data assimilation in crop models rely on observations retrieved from satellite  
285 monitoring of Earth's surface. Dorigo et al. (2007) [2] covered methods used to derive canopy  
286 state variables from optical remote sensing data in the visible to near-infrared and shortwave  
287 infrared regions. These methods either rely on statistical relationships between the spectral  
288 signature and the measured biophysical or biochemical properties of the canopy or they derive  
289 the states from the known behaviors of leaf reflectance and radiation propagation through the  
290 canopy. Both are used to obtain remote sensing products, which directly estimate the state for  
291 the final user. And both remote sensing products and reflectance itself, are used in assimilation.  
292 For those products, Huang et al. (2019a) [4] mention how guidelines for uncertainty  
293 quantification are still being established by the community and that many EO-derived products  
294 have poor or no uncertainty information available. Particularly for satellite-derived leaf area  
295 index (LAI) products, Fang et al. (2019) [41] also comment on how given the complexity  
296 associated to the retrieval process, a comprehensive quantitative assessment of the quality of  
297 LAI products is still missing. In the case of assimilating reflectance or albedo, the crop model  
298 is coupled with a radiative-transfer model (RTM), which allows for quantifying uncertainty in  
299 the measurements directly [42].

300 By assimilating products, several studies [26–28] are able to consider the observation as  
301 the same quantity as the state, which means the relationship between states and observations  
302 may be obtained by the unit matrix, simplifying the approach. The adverse effects of this choice

303 are not often discussed and the main example we found that mentions them comes from the  
304 study of De Wit and Van Diepen (2007) [23], which makes it explicit that the variance they  
305 ascribed to observations did not account for deficiencies in the conversion model itself, later  
306 concluding that the value they ascribed to the variance was indeed underestimated.

307       When measurements do not correspond directly to the state, filters require observation  
308 operators for the conversion. One observation operator often used is the RTM PROSAIL [42–  
309 45]. It combines the PROSPECT leaf optical properties model and the SAIL canopy  
310 bidirectional reflectance model, and is used for retrieval of vegetation biophysical properties  
311 [46]. Huang et al. (2019b) [42] used the RTM PROSAIL, arguing this is a good way to avoid  
312 the process of regional LAI retrieval, and Li et al. (2017) [43] used the PROSAIL model and  
313 characterized errors in the observations, pointing to values from 0.09 to 0.51 m<sup>2</sup> m<sup>-2</sup> of error in  
314 LAI in the different development stages of wheat. For those who develop their own  
315 measurement functions, they often establish them with empirical relationships and characterize  
316 their uncertainty based on field data [32,47]. Either in their case, in the case of using the  
317 PROSAIL or other RTMs or, for example, in the case of Kang and Özdoğan (2019) [8], who  
318 used a relationship between the Enhanced Vegetation Index extracted from Landsat images and  
319 field LAI observations derived from a global dataset with RMSE of 1.01m<sup>2</sup> m<sup>-2</sup> and MAE of  
320 0.81m<sup>2</sup> m<sup>-2</sup>, these metrics refer to the operator, which, as mentioned, may affect both estimates  
321 of state and covariance. For instance, depending on the quality of the observation operator, the  
322 conversion may lead to bias in the residual, and consequently, the updated estimate to the wrong  
323 value and, or by affecting the gain, to the wrong weight of the residuals in the new estimate.  
324 While observation uncertainties should be accounted for separately, these should not be  
325 disregarded when understanding the results.

326       As for observation uncertainties themselves, since these studies often refer to large areas,  
327 their estimates may be considered as the variability across fields. For instance, Zhao, Chen and

328 Shen (2013) [28] understood that neighboring pixels had similar uncertainties for the same  
329 period and used the variance among fields as uncertainty of remote sensing LAI. Huang et al.  
330 (2016) [27] stated that by random sampling their synthetic 30-m LAI series, the observational  
331 errors well for each 1-km grid cell were well-represented. For a time-series derived from  
332 Landsat, they obtained linear regressions between the observations and LAI values from the  
333 field-measured subplots and used the RMSE as observational errors. Kang and Özdoğan (2019)  
334 [8], on the other hand, assumed constant LAI observation variance at  $0.5 \text{ m}^2 \text{ m}^{-2}$ , which they  
335 claimed corresponds to the average variance of LAI within a county across the growing season.

336 Other than satellite retrieved data, there are other sources for observations to which error  
337 is ascribed in other ways. For instance, Linker and Ioslovich (2017) [22] and Ruíz-García et al.  
338 (2014) [38] used destructive measurements of the assimilated state. In the first case, the authors  
339 used direct measurements of aboveground biomass of potatoes and cotton and in the second  
340 case, of lettuces. As for non-destructive measurements, Linker and Ioslovich (2017) [22] also  
341 used pictures taken from 1.5 and 2 m above the crop to determine canopy cover. Since these  
342 were processed to obtain the fraction of the soil surface covered by the canopy, for the Aquacrop  
343 model this corresponded to a direct measurement of the state. On these cases, errors  
344 corresponded to variance from measurements. Data retrieved by unmanned aerial vehicles  
345 (UAVs) often have similar limitations as satellites regarding scale, but brings into discussions  
346 other aspects, particularly, as cameras are able to capture other types of data. For instance, Yu  
347 et al. (2020) [48] used field measured plant height as well as detected by UAVs and discussed  
348 the effects of multiple values ascribed to errors, arguing the trial-and-error procedure could  
349 provide a guideline when the true field observation error is unknown. Recently, Han et al.  
350 (2022) [49] commented on how, for smallholders, pictures could be a source of observations  
351 for assimilation and emphasized the need to properly characterize observation errors. They  
352 evaluated an approach in which the measurement and its error were estimated using the

353 probabilistic output of a convolutional neural network trained with pictures collected during  
354 growth using smartphones and labels obtained by destructive and non-destructive  
355 measurements.

356 Finally, one relevant aspect refers to how soil-crop systems may not have a constant value  
357 for the error. Nearing et al. (2012) [9] explain how the soil moisture observation uncertainty is  
358 variable throughout time, since measurement accuracy degrades as vegetation water content  
359 increases throughout the season. They ascribed to error measurement a value derived from the  
360 relationship between variance in the soil moisture retrieval and this fraction of plant population  
361 and plant biomass that corresponds to water. Lei et al. (2020) [13] evaluated a time-varying  
362 error for soil moisture observations as a function of LAI. They observed an overall  
363 improvement in soil moisture estimates, but also a somewhat less stable DA performance. Also  
364 for soil moisture, Mishra; Cruise and Mecikalski (2021) [34], chose a constant error for the  
365 observation, but they were aware that the errors in the sensors used behaved in contrasting ways  
366 over crop growth stages, and that this choice may have led to errors that were too low in the  
367 early growth season and larger later in the season. Lu et al. (2021) [29] used the multi-year  
368 average value of the daily standard deviation of the observations from the 4 soil moisture  
369 profiles. But for canopy cover, they noted the error varies dramatically during the growing  
370 season, with significant variability in the exponential growth stage and the decay period canopy  
371 cover, and only marginal when the canopy was near maximum. So, they assumed canopy cover  
372 observation error as dynamic, and the standard deviation of the samplings from the different  
373 zones on each sampling day was used separately. Li et al. (2017) [43] considered the standard  
374 deviation of the LAI observations as 10% of the measured value, based on their observations  
375 of LAI, and Curnel et al. (2011) [30] used a coefficient of variation to characterize uncertainty,  
376 thus ascribing to this hyperparameter of the filter a value that corresponded to a fraction of the  
377 observation. Belozerova (2023) [39] built a trend curve of LAI observations and used the

378 deviation from the trend curve as a proxy of measurement uncertainty, ascribing a different  
379 error estimate for each observation.

### 380 **2.3.2 Model estimates**

381 For Wallach and Thorburn (2017) [50], uncertainty means the distribution of the errors  
382 of prediction. By defining the model error ( $e$ ) as in Equation 1, these distributions may be  
383 ascertained in two different ways, depending on the predictor ( $f(X; \theta)$ ) being treated as fixed  
384 or random [51]. If the predictor is treated as fixed, the model error may be ascertained by  
385 hindcasts, determining the discrepancy between the prediction and an observed value ( $Y$ ). If it  
386 is not treated as fixed, each of its elements may then be treated as random variables, with several  
387 possible values and, therefore, uncertainty in the predictor may have as sources uncertainty in  
388 inputs ( $X$ ), model structure itself ( $f(X; \theta)$ ) and parameters ( $\theta$ ).

$$389 \quad e = Y - f(X; \theta) \quad \text{Equation 1}$$

390 In the case of Pellenq and Boulet (2004) [12], they had two situations, and the differences  
391 in model behavior, regarding soil moisture and biomass, required different approaches for  
392 determining sources of model uncertainty. When analyzing the effects of initial input values,  
393 they observed that for biomass, as the state value is propagated throughout growth, there is no  
394 compensation for previous errors, and errors in the estimates of initial conditions could impact  
395 the following behavior. And while for soil water, the reliance on previous values is lower, with  
396 shorter “memory” of the system, in the coupled case, the initial water content could strongly  
397 impact biomass evolution. As for crop model noise, they assumed there would be at least one  
398 parameter set in the ensemble that could satisfactorily reproduce natural conditions. So, they  
399 decided by generating ensembles ascribing uncertainty to parameters and to inputs. On the other  
400 hand, in the case of soil moisture, since it tends towards low variance and equilibrium, they  
401 suggested including model noise as well, which should be nonetheless calibrated to avoid the  
402 loss of model integrity. Nearing et al. (2012) [9] evaluated uncertainty in weather inputs,

403 through correlated perturbations in weather time-series. Their results were not conclusive as in  
404 one of their systems, the assimilation of LAI improved yield estimates, but not the exclusive  
405 assimilation of soil moisture.

406 Uncertain inputs also manifest through unusual events, which are often not included in  
407 models. Therefore, for some authors, an advantage of filter assimilation methods is that they  
408 can incorporate these dynamic changes [33]. For example, Hu et al. (2019) [52] improved  
409 sugarcane yield estimates by assimilating leaf area index into the SWAP-Wofost model, after  
410 the interference in LAI caused by artificial leaf stripping and natural storms, and in Zhao, Chen  
411 and Shen (2013) [28], the authors observed high errors when simulating yield for four regions  
412 in which meteorological disasters had occurred, which were then reduced to some extent by  
413 assimilating observations.

414 Calibration is an issue that is often mentioned regarding model errors, as it makes the  
415 model more consistent with the spatially limited field measurements and calculated uncertainty  
416 in parameters could be propagated through the model [4]. Kang and Özdoğan (2019) [8]  
417 commented on how, because over large areas, calibration is no longer specific for cultivar,  
418 sowing dates or management, model estimates become biased, which violates the assumptions  
419 of assimilation techniques that require model errors to have zero means and results in  
420 inefficiency of the method. It is then the case that before performing assimilation, models are  
421 frequently calibrated [4]. Lu et al. (2021) [29] believed the calibration standard was lower,  
422 aiming at having an ensemble of non-calibrated simulations that could capture the dynamics of  
423 key model states and that its spread reflected the model state variability. Their assimilation of  
424 canopy cover and soil moisture was able to improve yield when compared to the no-assimilation  
425 case. Following a similar premise, Fattori Junior et al (2022) [53] also assessed the effect of a  
426 non-genotype-specific calibration for multiple cultivars, and observed an overall improvement

427 in model estimates after assimilation in the non-calibrated model, using three assimilation  
428 techniques.

#### 429 **2.4 Variables**

430 In a way, the largest restrictions to performing data assimilation in crop models are which  
431 additional data is available and if the knowledge or ability of how to relate them to models'  
432 state variables exists. This is one reason why LAI, canopy cover and soil moisture are frequently  
433 explored as observations, as there are several satellite products available for them as well as  
434 they are often simulated by crop models. To counter availability restrictions, Luo et al. (2023)  
435 [5] point to how coupling multi-source remote sensing observations has become more explored  
436 and how some studies have shifted from univariate to multivariate assimilation to improve the  
437 robustness of crop yield estimates. But being able to perform data assimilation does not ensure  
438 that assimilation will be effective. As summarized by Lei et al. (2020) [13], the performance of  
439 any data assimilation algorithm is fundamentally related to the strength of the relationship  
440 between observations and model states.

441 For Mishra; Cruise and Mecikalski (2021) [34], assimilation of soil moisture, especially  
442 in irrigated areas, led to improvements in yield estimates, which is a very direct relationship,  
443 but for Ines et al. (2013) [26], they expected assimilation of soil moisture in the DSSAT-CSM-  
444 Maize model to update the rootzone soil moisture, affecting soil nitrogen and, therefore, yield.  
445 There is then no guarantee that the included observations will improve estimates. For instance,  
446 Linker and Ioslovich (2017) [22] discuss how since the Aquacrop model is water-driven, and  
447 as such, solar radiation is not considered explicitly, the effect of canopy cover on crop  
448 development may be underestimated. And if assimilation not improving the outcomes is  
449 undesirable, it should be noted that it could even have an adverse effect on the estimates,  
450 depending on how variables interact with each other. Tewes et al. (2020a) [54] argue that as  
451 model complexity rises, sequential update of only one or few state variables could threaten the

452 model's integrity and cause an undefined state of the model, such as when the simulation  
453 triggers a new module by reaching a threshold value, but the filter updates the estimate to a  
454 value lower than the threshold.

455 Time-averaged correlation has been suggested as not very helpful when determining best  
456 assimilating state variables by Nearing et al. (2012) [9]. In their experiments, they point to  
457 several cases, using different realistic uncertainty scenarios, in which high correlation is not  
458 connected to improvement in yield estimates. Nearing et al. (2018) [55] framed this discussion  
459 by relying on concepts of information theory, proposing a method to quantify how efficient data  
460 assimilation may be, through the quantification of information content on simulated model  
461 states and of the retrieval data relative to the imperfect evaluation data, and then measuring the  
462 fraction of this information that is extracted by a given DA implementation or algorithm.

## 463 **2.5 Timing and frequency**

464 An issue that interacts with which variable is going to be assimilated to improve an  
465 estimate is at what time of growth and how often should the estimate be updated. Frequently,  
466 the discussion is connected to at which moment of the cycle the observation available will be  
467 most informative. Dente et al. (2008) [47] evaluated the exclusion of one more precise image  
468 and observed that for wheat, within the conditions they observed, the data should include  
469 images from either the end of stem elongation stage or the beginning of heading, when the LAI  
470 reaches the maximum value. Timing of assimilation in wheat has been widely discussed  
471 [8,25,30,43,47] with some authors reaching the conclusion that images from the whole cycle  
472 presented the best results [8,43]. For sugarcane, on the other hand, Yu et al. (2020) [48]  
473 concluded that assimilation of height in the late period of the elongation stage, involving the  
474 maximum plant height, can be the most useful, without the need for its sampling over the whole  
475 development stage.

476 As remote sensing observations are often only available with large intervals between  
477 them, their assimilation allows for the model to adjust to the updates, but local assimilation of,  
478 for example, soil moisture, would present a different situation. Lu et al. (2021) [29] commented  
479 on how their use of local probes for monitoring soil moisture allowed for daily assimilation of  
480 this state, which likely improved their results. As crop systems models often present daily steps,  
481 it is not the case that assimilation would be performed in more frequent intervals, but in other  
482 contexts, such as weather forecasts, it has been argued that very frequent updates could insert  
483 noise in models, degrading forecasts [56].

### 484 **3 MATERIALS AND METHODS**

#### 485 **3.1 Data sources**

486 Environmental data collection was performed in research greenhouses cultivated with  
487 tomatoes and refer to photosynthetically active radiation and air temperature from three growth  
488 cycles. The first cycle took place from Jul/2019 to Oct/2019 (Exp 1), the second, from  
489 Nov/2020 to Feb/2021 (Exp 2) and the third, from Mar/2021 to Jun/2021 (Exp 3). Dry mass  
490 from aboveground plants' organs and leaf area index from destructive analyses of one tomato  
491 growth cycle (Exp 3) were also collected for model calibration. Data is publicly available  
492 [57,58].

#### 493 **3.2 Crop models**

494 With the environmental data from greenhouses, we simulated growth using the Reduced  
495 State Tomgro model (RT) [15] and the Vanthoor model (VM) [59]. We performed assimilation  
496 in the RT using observations obtained by simulation with both models, as detailed in section  
497 3.3. Because we focus on the RT model, a brief explanation on how it calculates fruit biomass  
498 is warranted. In the RT model, fruit biomass (Equation 1) is obtained directly from the balance  
499 between photosynthesis and respiration ( $GR_{net}$ , i.e., net aboveground biomass growth rate),

500 which is affected by suboptimal higher ( $g(T_{\text{daytime}})$ ) and lower temperatures ( $f_F(T_d)$ ), as well as  
 501 the maximum partitioning of new growth to fruit ( $\alpha_F$ ). From fruit biomass, another function of  
 502 temperature  $D_F(T_d)$  impacts the conversion of fruit biomass ( $W_F$ ) into mature fruit biomass  
 503 ( $W_M$ ) (Equation 2). In Equation 1,  $\vartheta$  and  $N_{FF}$  are parameters connected to the transition between  
 504 vegetative and reproductive stages and  $N$  is the number of nodes.

$$505 \quad \frac{dW_F}{dt} = GR_{net} \cdot \alpha_F \cdot f_F(T_d) \cdot [1 - e^{\vartheta - (N - N_{FF})}] \cdot g(T_{\text{daytime}}) \quad \text{Equation 2}$$

$$506 \quad \frac{dW_M}{dt} = D_F(T_d) \cdot (W_F - W_M) \quad \text{Equation 3}$$

507 For assimilation, RT model was used without local calibration, i.e., with parameters  
 508 obtained in the original experiment in Gainesville. For obtaining the artificial observations,  
 509 calibration was performed in the RT and in the VM through minimizing the relative squared  
 510 error of data obtained in the field and models' estimates through growth. Parameters values for  
 511 the Reduced State Tomgro model are presented in Supplementary Table A1.

### 512 3.3 Data assimilation

513 From the elements presented in Section 2.2, we chose two techniques, the Ensemble  
 514 Kalman Filter (EnKF), and the Unscented Kalman Filter (UKF). We evaluated the impacts of  
 515 different approaches for structuring model uncertainty when performing data assimilation for  
 516 improving yield estimates. Ground truth values corresponded to the simulations performed in  
 517 each of the three environments with the calibrated Reduced Tomgro.

- 518 • Two assimilated state variables: Fruit dry weight ( $W_f$ ) and Mature fruit dry weight  
 519 ( $W_m$ ).
- 520 • Two sources of observations: one (Case 1) in which three noise levels (10%, 30% and  
 521 50%) were ascribed to the simulations of the calibrated Reduced Tomgro ( $X_{\text{truth}}$ ) and one  
 522 (Case 2) in which calibrated Vanthoor model was used for simulations. While a 50% noise  
 523 level could seem excessive, it should be remarked that it could comprise the error from the

524 observation as well as the observation operator. In Case 1, the level multiplied by the  
525 observation was treated as the standard deviation of a normal distribution from which the  
526 perturbation was sampled (Equation 4), leading to the artificial observation ( $Y_{\text{artif}}$ ). Case 2  
527 was proposed as another artificial data source, but one in which the noise level was not  
528 chosen, similar to what would happen with observations retrieved from cameras, for  
529 example. Case 2 was not explored through all combinations below, but only for the scenarios  
530 with best performance for the more similar noise level of Case 1.

$$531 \quad Y_{\text{artif}_i} = X_{\text{truth}_i} + N(0, X_{\text{truth}_i} * \text{Noise}) \quad \text{Equation 4}$$

532 • Uncertainty in crop model: UKF requires determining a value for uncertainty in model  
533 estimates. Since assimilation was performed in the non-calibrated Reduced Tomgro model,  
534 we decided to ascribed these uncertainties as two variants of a relative error metric of the  
535 non-calibrated model (Table 1). The first is obtained by multiplying the estimate by the mean  
536 absolute percentage error of the model (MAPE, Equation 5, in which  $X_i$  is an estimated value  
537 from the non-calibrated model and  $Y_i$  is an observation measured through the cycle, also  
538 used for calibration) from the non-calibrated Reduced Tomgro model for the assimilated  
539 variable. This is denominated the fixed approach. The second approach, denominated  
540 variable, was obtained by multiplying the estimate by different relative errors through the  
541 cycle. Instead of the average value obtained in Equation 5, each relative absolute error (RAE)  
542 used in the calculation of MAPE is considered the as uncertainty associated with the  
543 estimates for that period (Equation 6). For the EnKF, as this uncertainty could be ascribed  
544 in four different ways, we made an assessment of the different approaches: 1. ascribing to  
545 the initial states the standard deviation of the observed initial values, 2. ascribing to a  
546 parameter, conditioned to which state variable would be assimilated (DFMax for mature fruit  
547 and alpha\_F for fruits, Supplementary Table A1), a perturbation of 10% of its value, 3.

548 ascribing to the hourly photosynthetically active radiation a perturbation of 10% of its value  
 549 and 4. ascribing the same values used for the UKF directly to the model state.

$$550 \quad MAPE = \frac{1}{n} \sum_i \frac{|Y_i - X_i|}{|X_i|}, X_i > 0 \quad \text{Equation 5}$$

$$551 \quad RAE = \frac{|Y_i - X_i|}{|X_i|} \quad \text{Equation 6}$$

552       • Uncertainty in observations: In Case 1, the noise level multiplied by the observation  
 553 was treated as treated as the uncertainty ( $R_i$ ) ascribed to that observation (Equation 7). In  
 554 Case 2, we ascribed the normalized root mean squared error from the calibrated Vanthoor  
 555 model for the assimilated variable, either using the RAE of the different observations in one  
 556 day or MAPE of the whole cycle (Table 1). In modes 2 and 3 of the EnKF uncertainty  
 557 assessment, as these perturbations affect the model difference equation output, instead of the  
 558 state variable itself, the uncertainty ascribed to observations should take this into account, or  
 559 variances in the filter will not be connected to the same quantity. To do so, in Case 1, we  
 560 defined the uncertainty as the difference between the current observation and its previous  
 561 value, multiplied by the respective noise level (Equation 8). In Case 2, for simplicity, we  
 562 applied the RAE to the difference between the current artificial observation and the previous  
 563 one (Equation 9) for variable observation error and, in the fixed case, the value used was the  
 564 MAPE.

$$565 \quad R_i = \left( Y_{artif_i} \times Noise \right)^2 \quad \text{Equation 7}$$

$$566 \quad R_i = \left[ \left( Y_{artif_i} - Y_{artif_{i-1}} \right) \times Noise \right]^2 = (R_i - R_{i-1})^2 \quad \text{Equation 8}$$

$$567 \quad R_i = \left[ \left( Y_{artif_i} - Y_{artif_{i-1}} \right) \times RAE \right]^2 \quad \text{Equation 9}$$

568       • We subsampled the observations to determine the effect of frequency. Subsampling  
 569 used 50% and 10% of the data available in the cycle. We repeated the process 20 times to

570 avoid biasing the results due to sampling, and in one of the repetitions, sampling was  
 571 regularly spaced through the cycle while in the others, it was random.

572 • The number of elements in the Ensemble Kalman Filter was defined as 250, after  
 573 evaluation (results not shown).

574 Table 1. Errors ascribed to the filters as uncertainty estimates.

State variable	Simulation day	Model [%]		Observations (Case 2) [%]	
		Wf	Wm	Wf	Wm
Fixed – Non-calibrated model	All	81	65	43	37
	1-10	0.01*	0.01*	0.01*	0.01*
	11-27	0.01*	0.01*	0.01*	0.01*
	28-38	100	0.01*	164	26
Variable	39-52	94	0.01*	15	2010
	53-66	82	51	20	20
	67-90	66	68	3.8	38
	91-end	66	75	7.9	52

575 \*Placeholder to avoid 0 variance.

576 There are few examples of how to assess model uncertainty, so we chose a simple  
 577 approach of using a relative error metric that could be comparable to the noise applied. We  
 578 evaluated our approaches by calculating the daily absolute relative error through growth  
 579 (Equation 6). Our focus on evaluating daily results is related to the indeterminate growth.  
 580 Differently from other crops in which one value is ascribed to yield, harvest for indeterminate  
 581 crops is continuous, and therefore, model errors through the growth cycle affect estimates along  
 582 harvests. Since the excess of zeros from the vegetative phase could skew these results, they  
 583 were not included in the calculation. We also show mean error (Equation 10) in order to discuss  
 584 bias.

$$585 \quad ME = Y_i - X_i \quad \text{Equation 10}$$

586 The code for the crop models was written in python and difference equations were  
 587 integrated by the Euler method. Filtering used the python filterpy library<sup>1</sup>, in which the

<sup>1</sup> <https://github.com/rllabbe/filterpy>

588 ensemble Kalman filter function was slightly modified to accommodate the multiple  
589 approaches for generating the ensemble. Data preparation for running simulations and  
590 simulation and assimilation results were processed using R. All code used in this study, is  
591 available in an online repository [60].

## 592 **4 RESULTS AND DISCUSSION**

593 We have identified in the Background section that even when the problem is well  
594 established, ascribing the covariances of filters' parameters is performed in multiple ways. In  
595 our evaluation of strategies to determine how to ascribe uncertainty to model and observations,  
596 we aimed at observing how imperfect measurements can allow for improvements on estimates  
597 of greenhouse tomato yield, when compared to using the model without calibration (Open  
598 Loop).

### 599 **4.1 Assimilation variable**

600 The first aspect we can comment on is the effect of assimilating an observation that is  
601 different from the target, i.e., the variable for which the improvement is desired. In this case  
602 study, Open Loop simulations severely underestimated the truth (Figure 1), but followed its  
603 same trend of largest estimates for Exp 2, which was conducted during spring-summer. Since  
604 the artificial observations of Case 1 followed the trends in the truth, relying on them to update  
605 the state would lead to increasing fruit biomass, which was observed. However, assimilation of  
606 fruits' observations ( $W_f$ ) in general led to an overestimation of yield, which for the lowest noise  
607 level, only slightly reduced the absolute errors in yield ( $W_m$ ) estimates — whenever it did  
608 reduce the error —, when compared to the model without calibration. Table 2 shows mean  
609 errors, to make explicit the differences in over and underestimation caused by assimilation, but  
610 improvement in absolute errors is highlighted in bold. On the other hand, assimilation of mature  
611 fruits' observations ( $W_m$ ) led to improvements for all experiments.

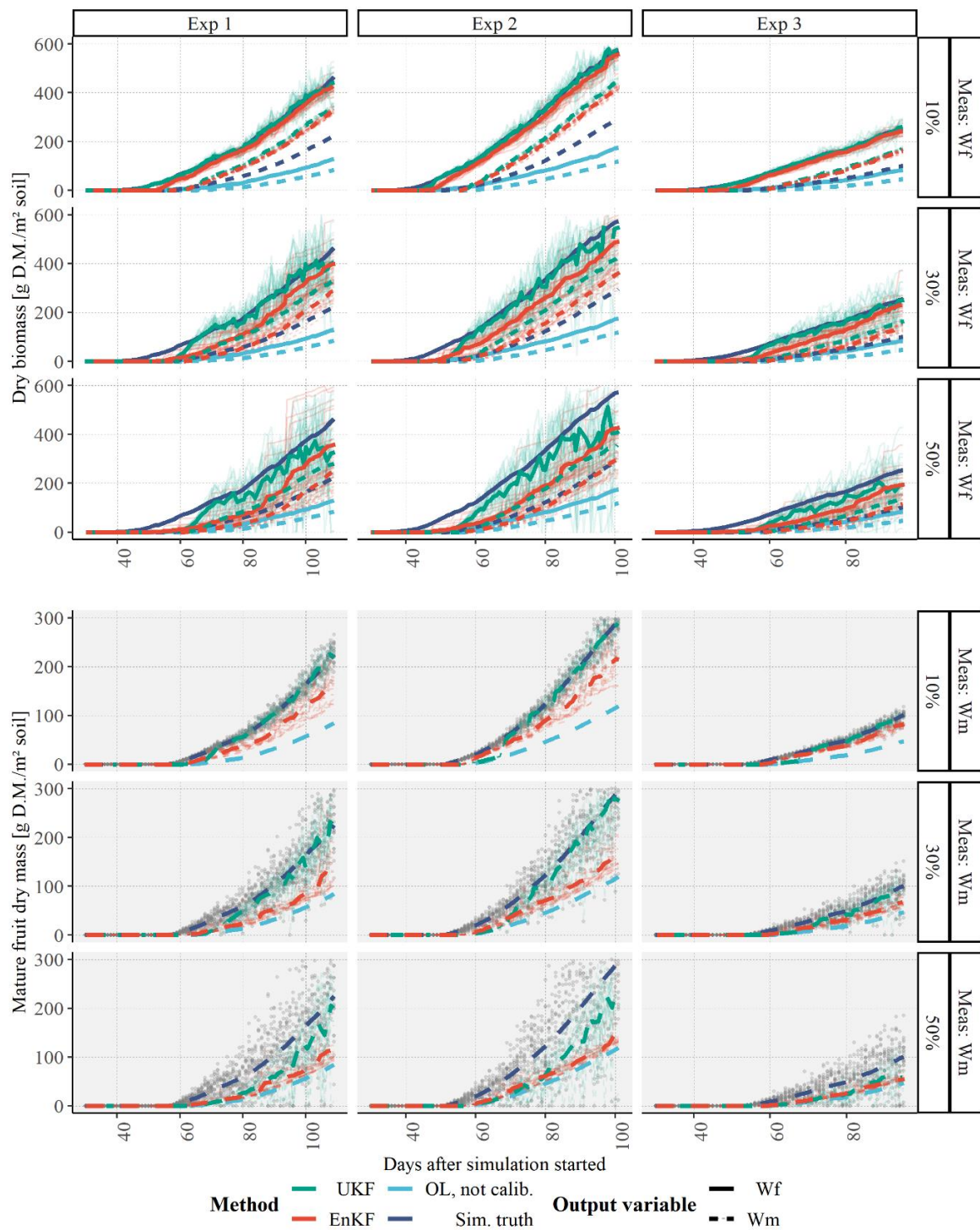
612

613 Table 2. Mean error (after fruit appearance) of mature fruit biomass with and without assimilation, using  
 614 the variable approach for observation (only Case 2) and for model uncertainties (both cases), with  
 615 simulated observations of fruit biomass (Wf) and mature fruit biomass (Wm). Bold numbers correspond  
 616 to the cases in which the absolute value is lower than the case without assimilation.

Case	Noise level	Assimilated variable	Filter	Exp 1	Exp 2	Exp 3	
No assimilation				-29.0	-36.6	-11.5	
1	10 %	Wf	EnKF	<b>21.1</b>	<b>29.2</b>	<b>11.1</b>	
			UKF	<b>27.3</b>	37.2	13.7	
		Wm	EnKF	<b>-13.1</b>	<b>-16.3</b>	<b>-4.02</b>	
			UKF	<b>-1.42</b>	<b>-2.94</b>	<b>-1.59</b>	
		30 %	Wf	EnKF	<b>5.75</b>	<b>13.0</b>	<b>4.41</b>
				UKF	<b>25.7</b>	<b>34.0</b>	12.3
	Wm		EnKF	<b>-20.8</b>	<b>-26.0</b>	<b>-6.90</b>	
			UKF	<b>-4.89</b>	<b>-7.60</b>	<b>-3.49</b>	
	50 %		Wf	EnKF	<b>-5.35</b>	<b>-5.77</b>	<b>-1.12</b>
				UKF	<b>14.3</b>	<b>20.1</b>	<b>5.71</b>
		Wm	EnKF	<b>-23.2</b>	<b>-30.6</b>	<b>-8.89</b>	
			UKF	<b>-14.1</b>	<b>-21.2</b>	<b>-8.04</b>	
2		-	Wf	EnKF	<b>-14.7</b>	<b>-29.6</b>	<b>1.33</b>
				UKF			
	Wm		EnKF	<b>-26.8</b>	<b>-38.1</b>	<b>-8.9</b>	
			UKF				

617

618



619

620 Figure 1. Overview of data assimilation results. Growth curves [g m<sup>-2</sup>] for fruit (continuous line) and  
 621 mature fruit dry mass (dashed line) obtained by assimilation of observations of fruit dry biomass (Meas:  
 622 Wf) or mature fruit dry biomass (Meas: Wm), with different noise levels, in the Reduced Tomgro Model,  
 623 with the complete observation dataset for the three weather experiments and ascribing variable  
 624 uncertainty for both model and observations. The Ensemble Kalman Filter used Approach 2 (parameter  
 625 perturbation) for ensemble generation. Assimilation curves in lighter colors refer to each of the 20  
 626 repetitions of the experiment. The darker curve refers to the average result of the assimilation runs. Dots  
 627 refer to all observations used in the multiple runs. For better visibility, fruit mass observations were  
 628 truncated at 800 g m<sup>-2</sup>. The x-axis was truncated at 30 days since the previous period corresponds to the  
 629 vegetative stage.

630           The first result happened because improving  $W_f$  estimates could not ensure  $W_m$  being  
631 correctly estimated. The simulations from the non-calibrated model (OL) showed very close  
632 estimates for  $W_f$  and  $W_m$ , representing a maturity rate much larger than the one from simulated  
633 truth. This is a consequence of the  $W_m$  estimate depending on a parameter that differed in more  
634 than 100% from the non-calibrated to the truth scenarios (Supplementary Table A1). The  
635 simulated truth also pointed to much larger overall biomass values than the estimates obtained  
636 by the non-calibrated model. So, while the model previously underestimated  $W_m$ , assimilation  
637 led to an overestimation, since  $W_m$  was then obtained by the non-calibrated model with the  
638 larger parameter, and based on a much larger value of  $W_f$ , as updated by the filter. This is  
639 similar to the problem described by Kang and Özdoğan (2019) [8] as error inconsistency.  
640 Interestingly, the largest noise in measurements allowed for model estimates to be more  
641 explored by the filter, so the process led to improved estimates by averaging the higher and  
642 lower estimates of  $W_f$ .

643           On the other hand, since assimilation of  $W_m$  itself did not depend on the step of the model  
644 processing the updated value, improvements, in particular for lower noise levels, are more  
645 noticeable. This effect is largely connected to the relationships between uncertainties as used  
646 by the Kalman Filters. We see that in general, for the assimilation of  $W_m$ , the lower the noise  
647 level, the closer the estimates were brought to the truth. It is the case then that not always  
648 assimilation is going to improve results, and this outcome depends on how the model will use  
649 the updated value and on its sensitivity to this input, i.e., how much the estimate relies solely  
650 on the input.

651           An additional issue, that is obfuscated by assessing metrics only, is the behavior  
652 associated with the estimates. Directly updating the state, as is the case with the UKF, may lead  
653 to frequent non-monotonic behavior that is not compatible with plant growth. In Figure 1,  
654 although the average curve represents a smoothed result, individual curves, represented in

655 lighter colors, are very erratic, in particular for higher noise levels. There are two possibilities  
656 that could attenuate this issue. The first is the frequency of assimilation. When Torres-  
657 Monsivais et al. (2017) [37] assessed the performance of the UKF in LAI assimilation with the  
658 RT, it seems that because they used fewer observations, the results they show do not lead to  
659 unreasonable curves, similar to the cases of updates performed with satellite imagery. The effect  
660 of frequent observation assimilation is further discussed on section 4.5. The second is the source  
661 of error in observations. In the example presented, the effect was amplified by sampling  
662 observations from a normal distribution with zero mean but increasingly larger variances.  
663 Despite the variability observed in the assimilation of fruits, the erratic behavior is attenuated  
664 when the updated fruit biomass estimate is processed by the model to estimate mature fruit  
665 biomass, since the update occurs in the level of the daily increment.

666 Finally, there are trade-offs in the decision of which variable to assimilate. We chose in  
667 this study to simulate observations more directly connected to yield. This choice would still  
668 allow for using the crop model for forecasting, ensuring the starting point of these chosen  
669 variables is as correct as possible, but it nevertheless limits the advantage of exploring all the  
670 model's potential. As stated in the section 2.4, other variables are more often used either given  
671 data availability or how much they affect the desired state variable. Therefore, while updating  
672 mature fruit biomass directly gives improved updates, it does not take advantage of the models'  
673 interaction components and, for example, impacts on leaf area that could lead to a reduction in  
674 fruit biomass will only be detected whenever fruit biomass is itself affected.

## 675 **4.2 Noise level**

676 It could be said that it is pointless to assimilate observations that are known to be  
677 incorrect, but since every measurement include some sort of error, the discussion is on the  
678 threshold accepted. For instance, the overall relative root mean squared error of high resolution  
679 remote sensing data used as reference values for the leaf area index of crops used in the

680 validation of moderate resolution LAI products ranged from 2.1% to 37% with a median of  
681 22% [41]. In our case, visually, noise levels corresponding to 30% still reasonably represent the  
682 truth, but noise levels of 50% may lead to very unreasonable, non-monotonic, estimates. In our  
683 case, sampling was centered on the truth, so the fluctuations represent noise in measurements,  
684 but observation errors could also be caused by systematic bias, which we did not represent.

685 In this Case 1, observations were expected to improve estimates, since the model was not  
686 calibrated and observations followed the trend in the truth. We also expected that increasing  
687 noise would lead to deterioration of filter performance. Both happened for the assimilation of  
688 mature fruit observations. But as the noise in observation increases and this information is  
689 passed to the filter, along with the observation covariance, the model estimate is further  
690 explored by the filter. And when the errors are in opposite directions, which is the case of  
691 assimilation of the biomass of fruits, they compensate and the result is an overall improvement  
692 in mature fruit biomass estimate.

### 693 **4.3 Ensemble generation approach**

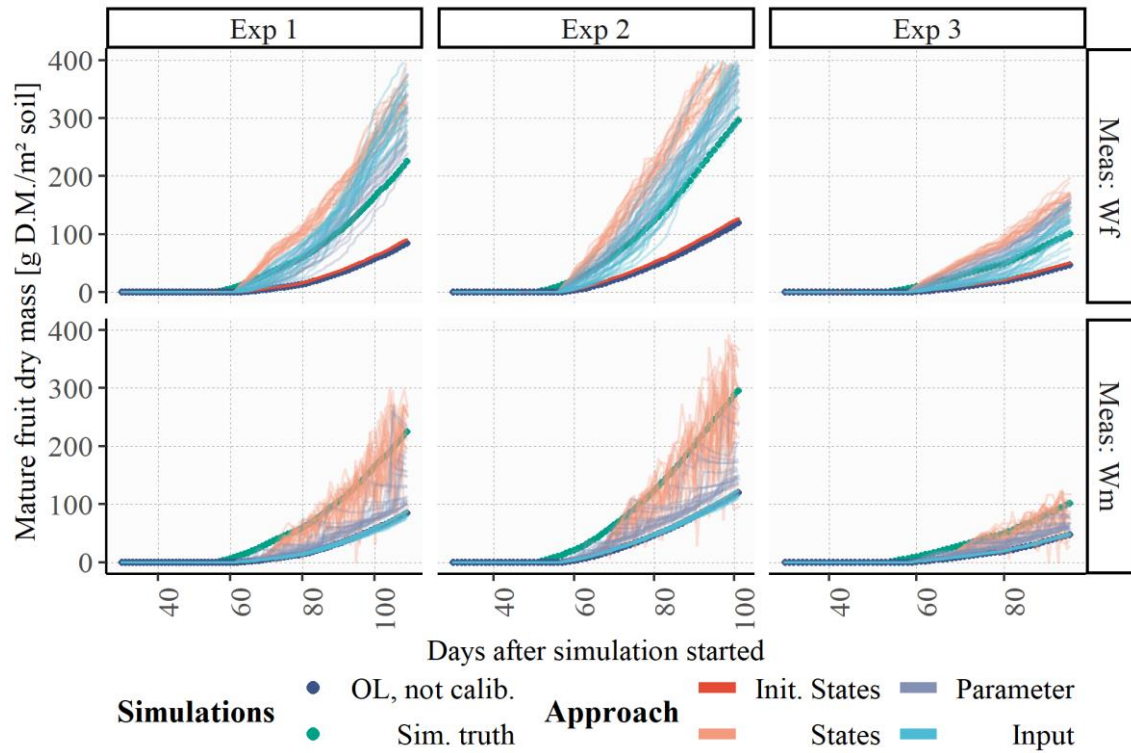
694 In Figure 1, we show only the results of the Ensemble Kalman Filter for the second  
695 approach of obtaining the ensemble described in section 3.3. We decided on further using this  
696 approach for the assessments after we observed the effects of the different approaches on yield  
697 (Figure 2) using the intermediate noise level. We noticed how, differently from directly  
698 updating the states either with the EnKF or the UKF, this approach led to reasonable results  
699 while not generating implausible curves even for the noisier observations, as discussed on  
700 section 4.1.

701 Furthermore, the Unscented Kalman Filter, when assimilating mature fruits, led to higher  
702 mature fruit biomass than fruit biomass (result not shown), which would not be realistic. This  
703 effect was not present in the EnKF as it relies more on model structure. Leaving the ensemble  
704 to be obtained by perturbing inputs and parameters likely lead to smoother results since they

705 affect the increment of the state variable and not the state itself. This means that, for observation  
706 uncertainty to be compatible with the variability generated within the ensemble, we needed to  
707 calculate uncertainties also based on the how these uncertainties affected the increments. This  
708 specific approach of associating the covariance of the observations with the magnitude of the  
709 increment is not explored in other studies.

710 On the other hand, changing only initial states or perturbing inputs did not improve the  
711 results as much. Changing initial states, while sometimes used, is less appropriate for a variable  
712 that will only change later in the cycle, differently from soil moisture, aboveground biomass,  
713 or leaf area index. To better assess this approach, perturbations could be performed at fruit  
714 appearance. Moreover, the choice of noise level ascribed to inputs likely led to less variability  
715 in the state variable being assimilated than the noise level that affected the parameters. This, in  
716 turn, led to lower covariance in the ensemble and more reliance in model estimates than in the  
717 observations. Similarly, even though we chose the parameters with highest values in a  
718 sensitivity analysis [61], the same 10% perturbation led to very different curve dispersion for  
719 fruits or for mature fruits.

720 It should also be noted that by leaving the uncertainty to perturbation, we imply that the  
721 estimate should be somewhere around the variability caused by this parameter or input, while  
722 ascribing it to the state considering model error, also carries an information with regard to the  
723 bias of the model. Albeit larger, it allows for the extra compensation, if needed.



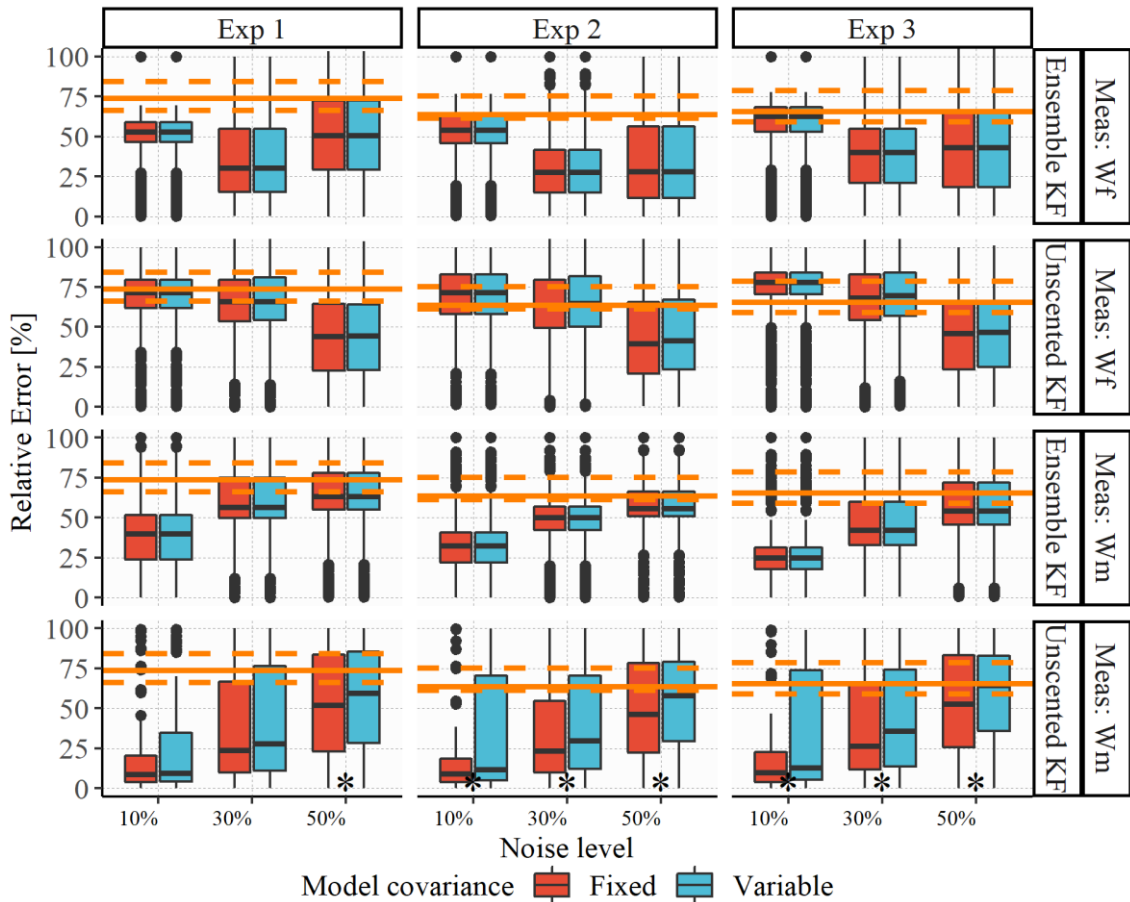
724

725 Figure 2. Outcomes for different ensemble approaches. Growth curves for the estimates of mature fruit  
 726 biomass [g m<sup>-2</sup>], by assimilation of fruit dry biomass (Meas: Wf) or mature fruit dry biomass (Meas:  
 727 Wm), using the Ensemble Kalman Filter with different approaches for ascribing uncertainty to the model:  
 728 to the initial state (Init. States), directly to the state variables (States), perturbing a parameter  
 729 (Parameter) or perturbing an input (Input). All curves for the 20 repetitions are shown, in each of the  
 730 three weather experiments, for the case of variable model uncertainty in simulations using 30% of noise  
 731 in observations.  
 732

#### 733 **4.4 Effect of variable model error**

734 After determining strategies for generating the ensemble, we assessed the effect of  
735 treating the noise level as fixed or variable. In this assessment, we meant to deal with an aspect  
736 of crop models that is that they often do not have constant variance [62]. The few studies that  
737 do not leave uncertainty to be determined in the ensemble define both a fixed value [37] or  
738 variable ones [22]. We did not observe a large difference between approaches (Figure 3), even  
739 though some are statistically different, likely because this effect was already mitigated by the  
740 use of relative values. Even though we present the results, there were, as expected, no  
741 differences between approaches in the assimilation using the EnKF, since for the ensemble  
742 generation method used, the covariance is derived from the perturbation in the parameters and  
743 is not an input. In the EnKF case, the model covariance naturally varies throughout the  
744 simulation.

745 For the UKF, the assimilation of fruits led to similar results between the approaches,  
746 within the same method and noise level, likely because the overall magnitudes of the  
747 uncertainties used either fixed or through growth (Table 1), are similar and the updated  
748 estimates are further modified by the model process. As previously discussed in section 4.1, the  
749 cases in which there was improvement in the estimates occur for the highest noise levels in  
750 observations. For the assimilation of mature fruit biomass, overall, the UKF was sensitive to  
751 the differences in covariance and even though the median error is similar, the variable approach  
752 frequently led to higher errors. These errors may be connected to small differences during  
753 mature fruit appearance, but are nonetheless quantified as high relative errors.



755 Figure 3. Assessment of the error in using different model covariance approaches. Relative errors for  
 756 daily estimates of mature fruit dry mass obtained by assimilation of artificial observations of fruit dry  
 757 biomass (Meas: Wf) or mature fruit dry biomass (Meas: Wm), obtained by different degrees of  
 758 perturbations in the outputs of the calibrated Reduced Tomgro model (noise levels 10%, 30% and 50%),  
 759 through the whole cycle. The results refer to three weather conditions, with two different approaches of  
 760 assigning uncertainty to the model, using both the Unscented and the Ensemble Kalman Filters.  
 761 Horizontal orange lines refer to the relative errors of the Reduced Tomgro model in estimating mature  
 762 fruits without assimilation: full line corresponds to the median and dashed lines to the 25th and 75th  
 763 percentiles. Y-axis is truncated at 100%. Asterisk corresponds to different distributions using the  
 764 Kolmogorov-Smirnov test with a 0.05 significance level.

#### 765 **4.5 Frequency of assimilation**

766 Assimilation frequency may be considered complementary to the acceptable noise level  
767 in observations, since assimilating an observation very frequently may not allow for the model  
768 to have an input in the estimates. In our example, this happens, counterintuitively, to the low  
769 noise level in the assimilation of fruits. We commented on section 4.1 how assimilating fruit  
770 observations overestimates mature fruit estimates. Therefore, the more frequent assimilation of  
771 them lead to increasing the error in yield estimates. When the noise increases, the opposite is  
772 true, and because the filter relies more on the model, the more frequent assimilation of these  
773 observations lead to a better result.

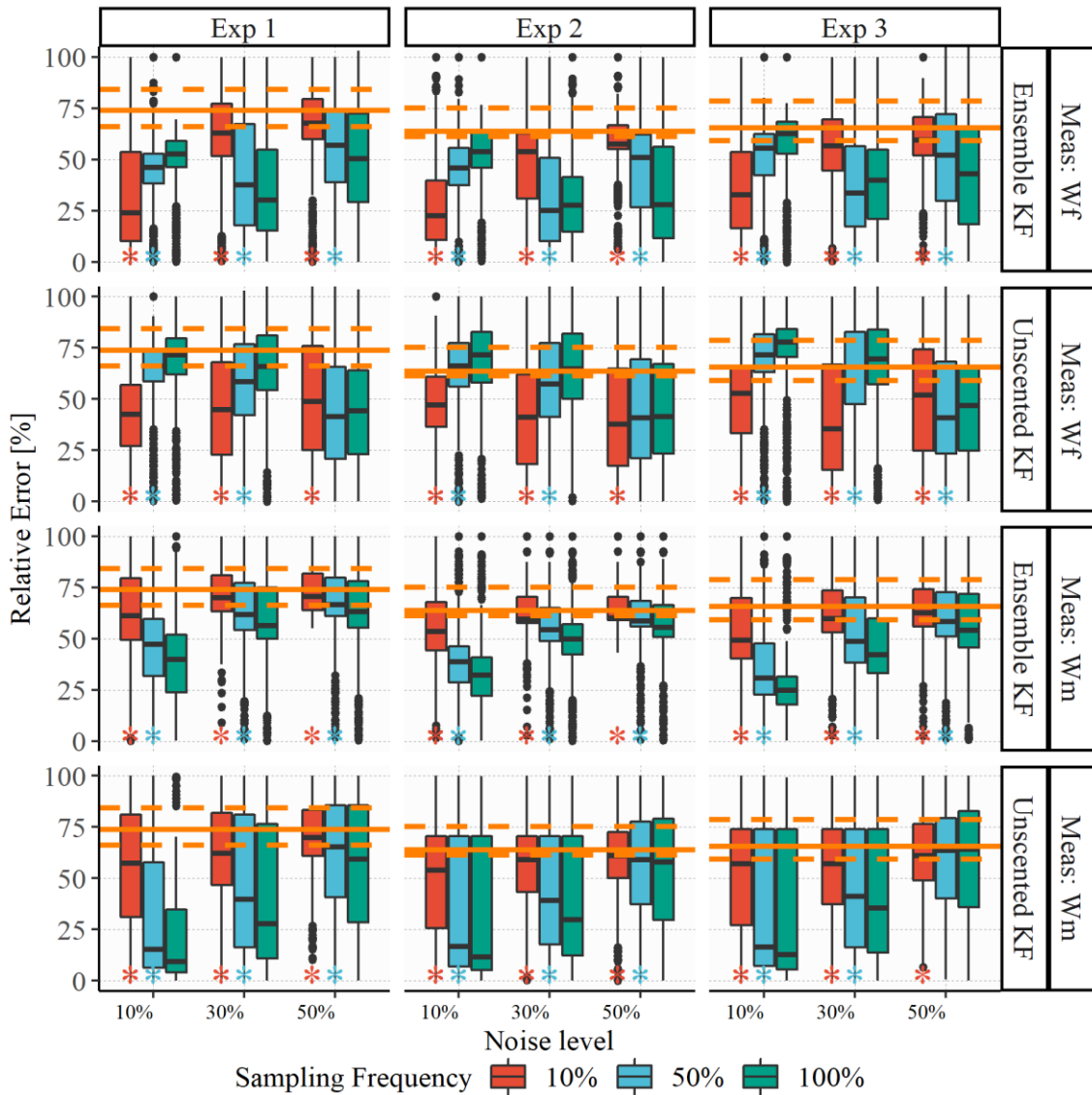
774 For the assimilation of mature fruits, we had already seen (section 4.2) that the  
775 assimilation of observations with the lowest noise levels led estimates to be closer to the truth,  
776 but the magnitude of the improvement depends on the covariance associated with model  
777 estimates (Figure 4). For the EnKF, the covariance generated on the ensemble seems lower than  
778 the one ascribed to the UKF so, as the noise in the observations increases, observations are less  
779 explored by the EnKF than by the UKF. Therefore, for the EnKF, reducing the frequency has a  
780 more pronounced effect when the noise level is the lowest, but less so when it increases.

781 The performance of the UKF follows overall the same pattern, but the covariance ascribed  
782 to the model allows the filter to explore more of the observations even with higher noise levels.  
783 So the effects of more frequent assimilation of fruit biomass leading to an increase in the error  
784 of yield estimates and of increasing median errors with fewer observations of mature fruit  
785 biomass occur up to the noise level of 30%.

786 By sampling twenty times randomly we do not assess the effect of timing of observations,  
787 but we can discuss the usefulness of continuous monitoring. In this example, for the highest  
788 noise level, assimilation with half the observations led to very similar results, in particular for  
789 the assimilation of mature fruit observations. This result is interesting when connected to  
790 processing capacity. For instance, if the observations are obtained by pictures of plants growing,

791 there would be no need for obtaining, storing, and extracting the related biomass from them  
792 every day.

793



794

795 Figure 4. Sampling frequency effect on assimilation. Relative errors for daily estimates of mature fruit  
 796 dry mass obtained by assimilation of artificial observations of fruit dry biomass (Meas: Wf) or mature  
 797 fruit dry biomass (Meas: Wm), obtained by different degrees of perturbations in the outputs of the  
 798 calibrated Reduced Tomgro model (noise levels 10%, 30% and 50%), through the whole cycle. The  
 799 results refer to three weather conditions, with different fractions of the complete observation dataset,  
 800 using both the Unscented and the Ensemble Kalman Filters. Horizontal orange lines refer to the relative  
 801 errors of the Reduced Tomgro model in estimating mature fruits without assimilation: full line  
 802 corresponds to the median and dashed lines to the 25th and 75th percentiles. Y-axis is truncated at 100%.  
 803 Asterisk corresponds to different distributions using the Kolmogorov-Smirnov test with a 0.05  
 804 significance level.

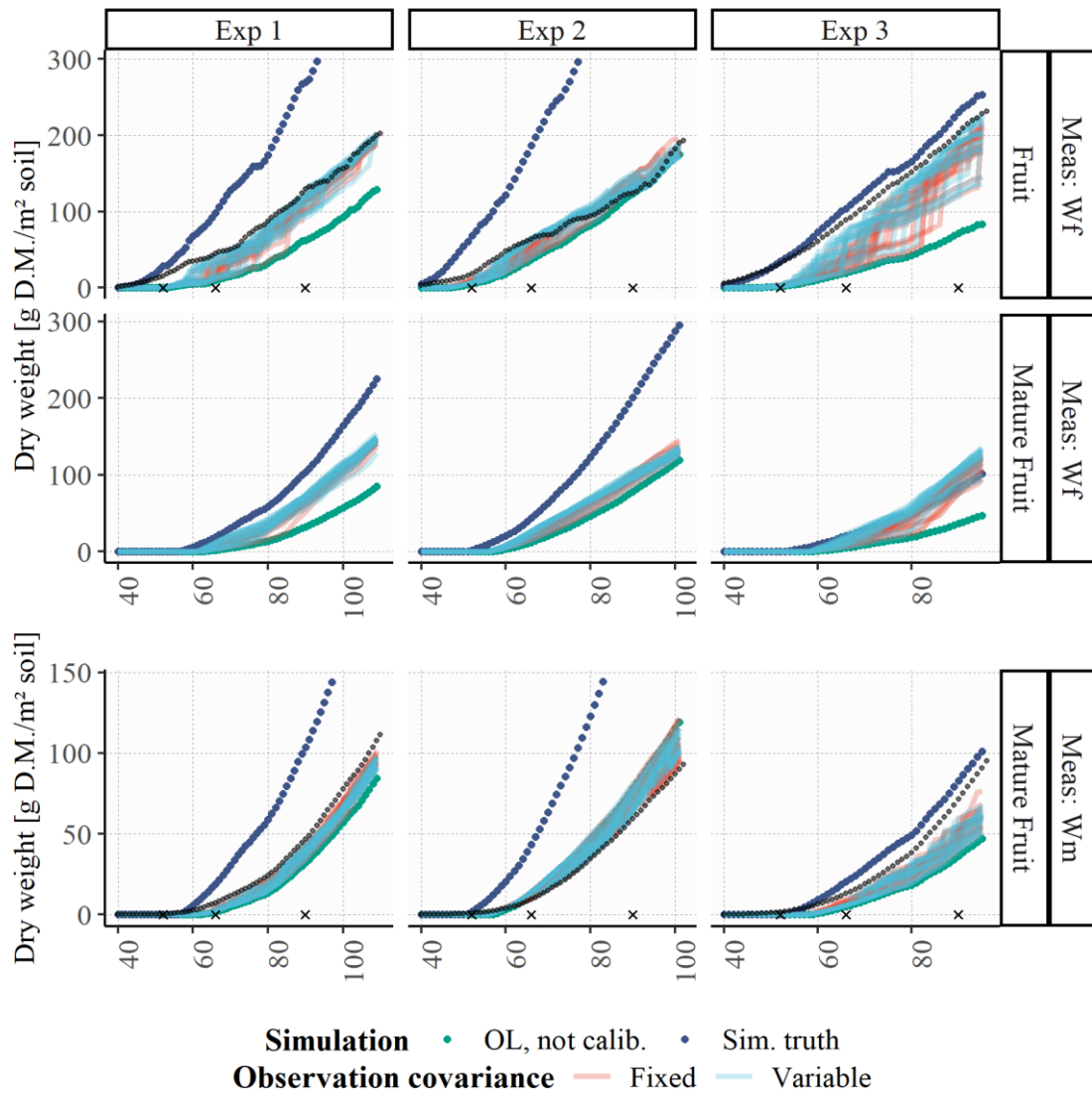
#### 805 **4.6 Different source for observations**

806 In this example, observations were obtained by simulation using the calibrated Vanthoor  
807 model. From the previous results, given its more stable performance, we only use the EnKF,  
808 which also allows for not having to choose the covariance behavior through the cycle. We again  
809 chose the approach of ensemble generation by using perturbation of parameters. Since in this  
810 case the uncertainty on observations is not by design, the covariance ascribed to them was also  
811 evaluated as variable through the cycle or fixed. While we could assess this case without  
812 repetitions associated with the observations, since they are simulated instead of obtained by  
813 adding noise, we decided to use 10% of observations to make more visible the differences in  
814 the two observation covariance approaches, thus leading to repeating the procedure to account  
815 for variability in sampling.

816 This is a scenario in which both model and observations underestimate the truth (Figure  
817 5), leading to the high errors seen in Table 2. But in all examples, the observation covariance  
818 ascribed was such that observations are quite explored by the filter, which also resulted in the  
819 improvement of the estimates. The exception occurs during fruit appearance, when the updated  
820 estimates are much closer to the ones obtained by the model. For the assimilation of fruits, with  
821 both approaches of ascribing the covariance, this is quite visible before the first date in which  
822 the covariance changes, marked by an 'x'. For the assimilation of mature fruits, this shift  
823 happens at the second date, more visibly in Exp 3.

824 We explored the approach of scaling the uncertainty in the observations by the period to  
825 which they refer, observing that without it, the gain would always be too low. By scaling, in all  
826 three experiments, for both approaches in the assimilation of fruits, we observed gain values  
827 ranging from 0 to almost 1, varying through the cycle. We mostly observed no difference  
828 between varying or fixing the covariance in the observations. Even the seemingly high fixed  
829 values ascribed (43% and 37%, Table 1) were apparently often of a compatible magnitude to  
830 the covariance generated by the ensemble.

831           By using fewer observations, we more clearly see the shifts in estimates caused by  
832 assimilation. After a shift in the magnitude, the Open Loop curve no longer represents model  
833 estimates, since the following estimates are based on the shifted updated value. This explains  
834 why, in Exp 2, some estimates are larger than both observation and open loop estimates.  
835



836

837 Figure 5. Assimilation results considering a different source for observations. Growth curves for fruit  
838 and mature fruit dry mass obtained by assimilation of fruit dry biomass (Meas: Wf) and for mature fruit  
839 dry biomass by assimilation of mature fruit dry biomass (Meas: Wm). Observations correspond to  
840 estimates of the Vanthoor model, using the Ensemble Kalman Filter (EnKF) with subsamples of 10%  
841 of the observation dataset for the three weather experiments and ascribing variable uncertainty for both  
842 model and observations and only to model. The x-axis was truncated at 40 days, since the previous  
843 period corresponds to the vegetative stage. Curves refer to all 20 repetitions of the experiment. For better  
844 visibility, fruit mass observations were truncated at 300 g m<sup>-2</sup> in the upper panels and at 150 g m<sup>-2</sup> in the  
845 lower panels.  
846

## 847 **5 FINAL REMARKS AND CONCLUSION**

848         The recently published reviews help to quantify and better understand the prevalent  
849 approaches of remote sensing assimilation into crop models, but when the specific application  
850 is different in all aspects including which models, observations and state variables are to be  
851 used, there are practical decisions that go beyond what has been discussed. Our goal in this  
852 study was to contextualize and apply data assimilation in the context of protected environments.  
853 These environments are used to grow different crops, e.g. horticultural or ornamental, which  
854 entails new models and new data sources. These data sources could be connected to multiple  
855 variables represented by crop models, free from the previous restrictions of what satellite  
856 imagery could provide. They could, for instance, rely on digital images to estimate either fruit  
857 mass or leaf area. This would also have implications in the frequency, which would no longer  
858 be restricted to satellites temporal resolution. But not only it is unclear which new variables  
859 could be useful, but also how to ascribe uncertainty to them would have to be thought through,  
860 since filter uncertainty parameter choices really impacts outcomes. And as these elements  
861 interact, there were many aspects to be discussed.

862         Giving meaning to filters' hyperparameters is a choice, as they could be tuned to obtain  
863 the best outcome [20,38]. But recent discussions in the crop modeling community have been  
864 moving from strictly data driven approaches towards hybrid ones [63] and the need for machine  
865 learning models to explore the knowledge constraints present in crop models has been  
866 emphasized [64,65]. For parameter calibration, instead of blind sensitivity analysis followed by  
867 optimization, the community has been proposing a mixture of expert knowledge in parameter  
868 and bound selection, followed by optimization using mathematical criteria (AIC and loss  
869 function) [66,67]. Therefore, while no meaning could lead to better outcomes, they would also  
870 hinder understandability in the process. We focused on approaching explainable ways to  
871 ascribing uncertainty to filters. One takeaway from our review and analysis is that observation  
872 covariances should not be fixed values. Kalman filter methods are an optimized approach for

873 performing a weighted average, in which the weights are related to the covariance of each  
874 estimate. Since errors grow in magnitude through the cycle, the process is more informed if  
875 covariances can vary with the magnitude of the observations and estimates, which naturally  
876 occurs in the Ensemble Kalman Filter. Ascribing covariance values as a proportion of the  
877 magnitude of estimates or observations can mitigate this issue.

878 We also noted how since these models work at the difference step, perturbation of  
879 elements of the equation to generate the ensemble leads to the need of scaling observation  
880 covariance. It is possible that this outcome is being achieved by using model uncertainty  
881 inflation, as suggested by Ines (2013) [26]. We noted in our experiments that, without scaling,  
882 the observation uncertainty was too large in comparison to the one generated in the ensemble,  
883 leading to gains almost always equal to zero. This was possible, however, because we directly  
884 assimilated observations. It's unclear how scaling could work when an observation operator is  
885 involved. This empirical result could be further investigated.

886 For model error, much of the discussion refers to bias, since many studies use the EnKF,  
887 which generates the model uncertainty. Using estimates from a non-calibrated model means  
888 more bias and uncertainty in the model estimate, so it is well-established that both should be  
889 reduced by parameter calibration to obtain a better estimate. Our example highlighted the aspect  
890 of updating the state itself being a weighted average which depended on the covariances  
891 ascribed both to model and observation, but that update of a different variable could be heavily  
892 affected by the relationship of the updated and the target variable.

893 Finally, we noted that which variable to assimilate is an open question for field data as  
894 well. Previous assessments with artificial data could be useful for avoiding trial-and-error ad-  
895 hoc studies with laborious data gathering steps. In a new context, in which there is little previous  
896 research pointing to which variables could be useful, choosing the variable means defining  
897 which data will be collected. In that sense, good understanding of the models is helpful. Our

898 study allowed for directly assessing the relationships between the assimilated variable and a  
899 parameter or another state, but this is often not possible, since the models are usually more  
900 complex and the relationships between variables are not so direct.

901 In part, extended state estimation is solving the issue by leveraging sensitivity analysis,  
902 so that at least one component of the model, i.e., parameters, are changed with assurance of  
903 impact on the target variable. Orlova and Linker (2023) [14] used sensitivity analysis  
904 immediately before the assimilation step, to account for changes in parameter importance  
905 through the growth cycle. This approach, however, still relies on how the model represents the  
906 process, which prevents the assimilation advantage of capturing processes not included in the  
907 model. It could be said that parameter would behave as dynamic, accommodating these  
908 processes, but in this case, they may lose their original meaning. Furthermore, the value would  
909 be identified within the process. To be able to choose which variable and through it, which data  
910 to collect, the analysis would have to be performed prior to assimilation. A sequential sensitivity  
911 analysis for multiple state variables [68] could allow for identifying which parameter impacts  
912 both the various state variables that could be assimilated as well as the target state variable,  
913 suggesting an interesting variable to assimilate.

914 Sensitivity analyses methods are well-established to characterize which elements impact  
915 an outcome the most. It focuses, however, on parameters, and effects from bias on other state  
916 variables and weather conditions are not included. Ines et al. (2013) [26] concluded that weather  
917 conditions expected during the growing season could provide information as to when a variable  
918 is best to be assimilated, and this would include a beneficial constraint in a sensitivity analyses  
919 across multiple years [61].

920 To address the two main points of how to characterize uncertainties and how to choose  
921 useful variables, it could be the case that protocols, such as those being proposed for calibration  
922 [67,69,70] could also be explored. At least a framework could be designed on how uncertainties

923 should be understood before moving into data gathering. The would be helpful both for  
924 practitioners that are now approaching the subject, but also for those that have already been  
925 using remote sensing observations, but with new models and crops.

## 926 **6 ACKNOWLEDGEMENTS**

927 This study was financed in part by the Coordenação de Aperfeiçoamento de Pessoal de  
928 Nível Superior - Brasil (CAPES) - Finance Code 001, by grant #2018/12050-6, São Paulo  
929 Research Foundation (FAPESP), and by CNPq (grant #308811/2019-4). The funding sources  
930 had no role in the study design; the collection, analysis, and interpretation of data; the writing  
931 of the report; or the decision to submit the article for publication.

## 932 **7 AUTHORS' CONTRIBUTIONS**

933 Monique Oliveira: Conceptualization, Methodology, Software, Investigation, Data Curation,  
934 Writing - Original Draft; Thais Zorzeto-Cesar: Resources, Writing - Review & Editing; Romis  
935 Attux: Writing - Review & Editing; Luiz Rodrigues: Writing - Review & Editing, Supervision,  
936 Funding acquisition

## 937 **8 CONFLICTS OF INTEREST**

938 The authors declare that there is no conflict of interest.

## 939 **9 REFERENCES**

- 940 [1] A. Fischer, L. Kergoat, G. Dedieu, Coupling Satellite Data with Vegetation Functional  
941 Models: Review of Different Approaches and Perspectives Suggested by the  
942 Assimilation Strategy, *Remote Sens. Rev.* 15 (1997) 283–303.  
943 <https://doi.org/10.1080/02757259709532343>.
- 944 [2] W.A. Dorigo, R. Zurita-Milla, A.J.W. de Wit, J. Brazile, R. Singh, M.E. Schaepman, A  
945 review on reflective remote sensing and data assimilation techniques for enhanced

- 946 agroecosystem modeling, *Int. J. Appl. Earth Obs. Geoinf.* 9 (2007) 165–193.  
947 <https://doi.org/10.1016/j.jag.2006.05.003>.
- 948 [3] X. Jin, L. Kumar, Z. Li, H. Feng, X. Xu, G. Yang, J. Wang, A review of data assimilation  
949 of remote sensing and crop models, *Eur. J. Agron.* 92 (2018) 141–152.  
950 <https://doi.org/10.1016/j.eja.2017.11.002>.
- 951 [4] J. Huang, J.L. Gómez-Dans, H. Huang, H. Ma, Q. Wu, P.E. Lewis, S. Liang, Z. Chen,  
952 J.-H. Xue, Y. Wu, F. Zhao, J. Wang, X. Xie, Assimilation of remote sensing into crop  
953 growth models: Current status and perspectives, *Agric. For. Meteorol.* 276–277 (2019)  
954 107609. <https://doi.org/10.1016/j.agrformet.2019.06.008>.
- 955 [5] L. Luo, S. Sun, J. Xue, Z. Gao, J. Zhao, Y. Yin, F. Gao, X. Luan, Crop yield estimation  
956 based on assimilation of crop models and remote sensing data: A systematic evaluation,  
957 *Agric. Syst.* 210 (2023) 103711. <https://doi.org/10.1016/j.agsy.2023.103711>.
- 958 [6] L. Liu, J. Yuan, L. Gong, X. Wang, X. Liu, Dynamic Fresh Weight Prediction of  
959 Substrate-Cultivated Lettuce Grown in a Solar Greenhouse Based on Phenotypic and  
960 Environmental Data, *Agriculture.* 12 (2022) 1959.  
961 <https://doi.org/10.3390/agriculture12111959>.
- 962 [7] T. Moon, D. Kim, S. Kwon, T.I. Ahn, J.E. Son, Non-Destructive Monitoring of Crop  
963 Fresh Weight and Leaf Area with a Simple Formula and a Convolutional Neural  
964 Network, *Sensors.* 22 (2022) 7728. <https://doi.org/10.3390/s22207728>.
- 965 [8] Y. Kang, M. Özdoğan, Field-level crop yield mapping with Landsat using a hierarchical  
966 data assimilation approach, *Remote Sens. Environ.* 228 (2019) 144–163.  
967 <https://doi.org/10.1016/J.RSE.2019.04.005>.
- 968 [9] G.S. Nearing, W.T. Crow, K.R. Thorp, M.S. Moran, R.H. Reichle, H. V. Gupta,  
969 Assimilating remote sensing observations of leaf area index and soil moisture for wheat  
970 yield estimates: An observing system simulation experiment, *Water Resour. Res.* 48

- 971 (2012). <https://doi.org/10.1029/2011WR011420>.
- 972 [10] J. Rong, H. Zhou, F. Zhang, T. Yuan, P. Wang, Tomato cluster detection and counting  
973 using improved YOLOv5 based on RGB-D fusion, *Comput. Electron. Agric.* 207 (2023)  
974 107741. <https://doi.org/10.1016/j.compag.2023.107741>.
- 975 [11] F. Zhang, Z. Lv, H. Zhang, J. Guo, J. Wang, T. Lu, L. Zhangzhong, Verification of  
976 improved YOLOX model in detection of greenhouse crop organs: Considering tomato  
977 as example, *Comput. Electron. Agric.* 205 (2023) 107582.  
978 <https://doi.org/10.1016/j.compag.2022.107582>.
- 979 [12] J. Pellenq, G. Boulet, A methodology to test the pertinence of remote-sensing data  
980 assimilation into vegetation models for water and energy exchange at the land surface,  
981 *Agronomie*. 24 (2004) 197–204. <https://doi.org/10.1051/agro:2004017>.
- 982 [13] F. Lei, W.T. Crow, W.P. Kustas, J. Dong, Y. Yang, K.R. Knipper, M.C. Anderson, F.  
983 Gao, C. Notarnicola, F. Greifeneder, L.M. McKee, J.G. Alfieri, C. Hain, N. Dokoozlian,  
984 Data assimilation of high-resolution thermal and radar remote sensing retrievals for soil  
985 moisture monitoring in a drip-irrigated vineyard, *Remote Sens. Environ.* 239 (2020)  
986 111622. <https://doi.org/10.1016/j.rse.2019.111622>.
- 987 [14] Y. Orlova, R. Linker, Data assimilation with sensitivity-based particle filter: A  
988 simulation study with AquaCrop, *Comput. Electron. Agric.* 204 (2023) 107538.  
989 <https://doi.org/10.1016/j.compag.2022.107538>.
- 990 [15] J.W. Jones, A. Kenig, C.E. Vallejos, Reduced state-variable tomato growth model,  
991 *Trans. ASAE*. 42 (1999) 255–265. <https://doi.org/10.13031/2013.13203>.
- 992 [16] F.W.T.P. De Vries, Phases of development of models, in: *Simul. Plant Growth Crop*  
993 *Prod.*, Pudoc, 1982: pp. 20–25.
- 994 [17] J.B. Passioura, Simulation models: Science, snake oil, education, or engineering?,  
995 *Agron. J.* 88 (1996) 690–694.

- 996 <https://doi.org/10.2134/agronj1996.00021962008800050002x>.
- 997 [18] J.W. Jones, J.M. Antle, B. Basso, K.J. Boote, R.T. Conant, I. Foster, H.C.J. Godfray, M.  
998 Herrero, R.E. Howitt, S. Janssen, B.A. Keating, R. Munoz-Carpena, C.H. Porter, C.  
999 Rosenzweig, T.R. Wheeler, Brief history of agricultural systems modeling, *Agric. Syst.*  
1000 155 (2017) 240–254. <https://doi.org/10.1016/j.agsy.2016.05.014>.
- 1001 [19] M. Vazifedoust, J.C. van Dam, W.G.M. Bastiaanssen, R.A. Feddes, Assimilation of  
1002 satellite data into agrohydrological models to improve crop yield forecasts, *Int. J. Remote*  
1003 *Sens.* 30 (2009) 2523–2545. <https://doi.org/10.1080/01431160802552769>.
- 1004 [20] Y. Chen, Z. Zhang, F. Tao, Improving regional winter wheat yield estimation through  
1005 assimilation of phenology and leaf area index from remote sensing data, *Eur. J. Agron.*  
1006 101 (2018) 163–173. <https://doi.org/10.1016/J.EJA.2018.09.006>.
- 1007 [21] Y. Chen, F. Tao, Improving the practicability of remote sensing data-assimilation-based  
1008 crop yield estimations over a large area using a spatial assimilation algorithm and  
1009 ensemble assimilation strategies, *Agric. For. Meteorol.* 291 (2020) 108082.  
1010 <https://doi.org/10.1016/j.agrformet.2020.108082>.
- 1011 [22] R. Linker, I. Ioslovich, Assimilation of canopy cover and biomass measurements in the  
1012 crop model AquaCrop, *Biosyst. Eng.* 162 (2017) 57–66.  
1013 <https://doi.org/10.1016/j.biosystemseng.2017.08.003>.
- 1014 [23] A.J.W. de Wit, C.A. van Diepen, Crop model data assimilation with the Ensemble  
1015 Kalman filter for improving regional crop yield forecasts, *Agric. For. Meteorol.* 146  
1016 (2007) 38–56. <https://doi.org/10.1016/j.agrformet.2007.05.004>.
- 1017 [24] M.P.G. De Oliveira, T.Q. Zorzeto-Cesar, R.R.D.F. Attux, L.H.A. Rodrigues, Can  
1018 accuracy issues of low-cost sensor measurements be overcome with data assimilation?,  
1019 *Eng. Agrícola.* 43 (2023) 2–8. [https://doi.org/10.1590/1809-4430-](https://doi.org/10.1590/1809-4430-eng.agric.v43n2e20220170/2023)  
1020 [eng.agric.v43n2e20220170/2023](https://doi.org/10.1590/1809-4430-eng.agric.v43n2e20220170/2023).

- 1021 [25] Y. Xie, P. Wang, X. Bai, J. Khan, S. Zhang, L. Li, L. Wang, Assimilation of the leaf area  
1022 index and vegetation temperature condition index for winter wheat yield estimation using  
1023 Landsat imagery and the CERES-Wheat model, *Agric. For. Meteorol.* 246 (2017) 194–  
1024 206. <https://doi.org/10.1016/J.AGRFORMET.2017.06.015>.
- 1025 [26] A.V.M. Ines, N.N. Das, J.W. Hansen, E.G. Njoku, Assimilation of remotely sensed soil  
1026 moisture and vegetation with a crop simulation model for maize yield prediction, *Remote*  
1027 *Sens. Environ.* 138 (2013) 149–164. <https://doi.org/10.1016/J.RSE.2013.07.018>.
- 1028 [27] J. Huang, F. Sedano, Y. Huang, H. Ma, X. Li, S. Liang, L. Tian, X. Zhang, J. Fan, W.  
1029 Wu, Assimilating a synthetic Kalman filter leaf area index series into the WOFOST  
1030 model to improve regional winter wheat yield estimation, *Agric. For. Meteorol.* 216  
1031 (2016) 188–202. <https://doi.org/10.1016/j.agrformet.2015.10.013>.
- 1032 [28] Y. Zhao, S. Chen, S. Shen, Assimilating remote sensing information with crop model  
1033 using Ensemble Kalman Filter for improving LAI monitoring and yield estimation, *Ecol.*  
1034 *Modell.* 270 (2013) 30–42. <https://doi.org/10.1016/j.ecolmodel.2013.08.016>.
- 1035 [29] Y. Lu, T.P. Chibarabada, M.G. Ziliani, J.K. Onema, M.F. McCabe, J. Sheffield,  
1036 Assimilation of soil moisture and canopy cover data improves maize simulation using an  
1037 under-calibrated crop model, *Agric. Water Manag.* 252 (2021) 106884.  
1038 <https://doi.org/10.1016/j.agwat.2021.106884>.
- 1039 [30] Y. Curnel, A.J.W. de Wit, G. Duveiller, P. Defourny, Potential performances of remotely  
1040 sensed LAI assimilation in WOFOST model based on an OSS Experiment, *Agric. For.*  
1041 *Meteorol.* 151 (2011) 1843–1855. <https://doi.org/10.1016/j.agrformet.2011.08.002>.
- 1042 [31] G. Burgers, P. Jan van Leeuwen, G. Evensen, Analysis Scheme in the Ensemble Kalman  
1043 Filter, *Mon. Weather Rev.* 126 (1998) 1719–1724. [https://doi.org/10.1175/1520-0493\(1998\)126<1719:ASITEK>2.0.CO;2](https://doi.org/10.1175/1520-0493(1998)126<1719:ASITEK>2.0.CO;2).
- 1044
- 1045 [32] T. Bai, S. Wang, W. Meng, N. Zhang, T. Wang, Y. Chen, B. Mercatoris, Assimilation

- 1046 of Remotely-Sensed LAI into WOFOST Model with the SUBPLEX Algorithm for  
1047 Improving the Field-Scale Jujube Yield Forecasts, *Remote Sens.* 11 (2019) 1945.  
1048 <https://doi.org/10.3390/rs11161945>.
- 1049 [33] Y. Li, Q. Zhou, J. Zhou, G. Zhang, C. Chen, J. Wang, Assimilating remote sensing  
1050 information into a coupled hydrology-crop growth model to estimate regional maize  
1051 yield in arid regions, *Ecol. Modell.* 291 (2014).  
1052 <https://doi.org/10.1016/j.ecolmodel.2014.07.013>.
- 1053 [34] V. Mishra, J.F. Cruise, J.R. Mecikalski, Assimilation of coupled microwave / thermal  
1054 infrared soil moisture profiles into a crop model for robust maize yield estimates over  
1055 Southeast United States, *Eur. J. Agron.* 123 (2021) 126208.  
1056 <https://doi.org/10.1016/j.eja.2020.126208>.
- 1057 [35] J. Yin, X. Zhan, Y. Zheng, C.R. Hain, J. Liu, L. Fang, Optimal ensemble size of ensemble  
1058 Kalman filter in sequential soil moisture data assimilation, *Geophys. Res. Lett.* 42 (2015)  
1059 6710–6715. <https://doi.org/10.1002/2015GL063366>.
- 1060 [36] M. Mansouri, B. Dumont, M.-F. Destain, Modeling and prediction of nonlinear  
1061 environmental system using Bayesian methods, *Comput. Electron. Agric.* 92 (2013) 16–  
1062 31. <https://doi.org/10.1016/j.compag.2012.12.013>.
- 1063 [37] J.C. Torres-Monsivais, I.L. López-Cruz, A. Ruíz-García, J.A. Ramírez-Arias, R.D. Peña-  
1064 Moreno, Data assimilation to improve states estimation of a dynamic greenhouse  
1065 tomatoes crop growth model, *Acta Hortic.* (2017) 433–440.  
1066 <https://doi.org/10.17660/ActaHortic.2017.1170.53>.
- 1067 [38] A. Ruíz-García, I.L. López-Cruz, A. Ramírez-Arias, E. Rico-Garcia, Modeling  
1068 uncertainty of greenhouse crop lettuce growth model using Kalman Filtering, *Acta*  
1069 *Hortic.* 1037 (2014) 361–368. <https://doi.org/10.17660/ActaHortic.2014.1037.44>.
- 1070 [39] O.D. Belozeroва, Enhancing WOFOST crop model with unscented Kalman filter

- 1071 assimilation of leaf area index, *Int. J. Image Data Fusion*. 00 (2023) 1–16.  
1072 <https://doi.org/10.1080/19479832.2023.2287037>.
- 1073 [40] D. Wallach, D. Makowski, J.W. Jones, F. Brun, Data Assimilation for Dynamic Models,  
1074 in: D. Wallach, D. Makowski, J.W. Jones, F. Brun (Eds.), *Work. with Dyn. Crop Model.*,  
1075 Third Edit, Elsevier, 2019: pp. 487–518. [https://doi.org/10.1016/B978-0-12-811756-](https://doi.org/10.1016/B978-0-12-811756-9.00014-9)  
1076 [9.00014-9](https://doi.org/10.1016/B978-0-12-811756-9.00014-9).
- 1077 [41] H. Fang, F. Baret, S. Plummer, G. Schaepman-Strub, An Overview of Global Leaf Area  
1078 Index (LAI): Methods, Products, Validation, and Applications, *Rev. Geophys.* 57 (2019)  
1079 739–799. <https://doi.org/10.1029/2018RG000608>.
- 1080 [42] J. Huang, H. Ma, F. Sedano, P. Lewis, S. Liang, Q. Wu, W. Su, X. Zhang, D. Zhu,  
1081 Evaluation of regional estimates of winter wheat yield by assimilating three remotely  
1082 sensed reflectance datasets into the coupled WOFOST–PROSAIL model, *Eur. J. Agron.*  
1083 102 (2019) 1–13. <https://doi.org/10.1016/J.EJA.2018.10.008>.
- 1084 [43] H. Li, Z. Chen, G. Liu, Z. Jiang, C. Huang, Improving Winter Wheat Yield Estimation  
1085 from the CERES-Wheat Model to Assimilate Leaf Area Index with Different  
1086 Assimilation Methods and Spatio-Temporal Scales, *Remote Sens.* 9 (2017) 190.  
1087 <https://doi.org/10.3390/rs9030190>.
- 1088 [44] L. Zhang, C.L. Guo, L.Y. Zhao, Y. Zhu, W.X. Cao, Y.C. Tian, T. Cheng, X. Wang,  
1089 Estimating wheat yield by integrating the WheatGrow and PROSAIL models, *F. Crop.*  
1090 *Res.* 192 (2016) 55–66. <https://doi.org/10.1016/j.fcr.2016.04.014>.
- 1091 [45] C. Guo, Y. Tang, J. Lu, Y. Zhu, W. Cao, T. Cheng, L. Zhang, Y. Tian, Predicting wheat  
1092 productivity: Integrating time series of vegetation indices into crop modeling via  
1093 sequential assimilation, *Agric. For. Meteorol.* 272–273 (2019) 69–80.  
1094 <https://doi.org/10.1016/J.AGRFORMET.2019.01.023>.
- 1095 [46] S. Jacquemoud, W. Verhoef, F. Baret, C. Bacour, P.J. Zarco-Tejada, G.P. Asner, C.

- 1096 François, S.L. Ustin, PROSPECT + SAIL models: A review of use for vegetation  
1097 characterization, *Remote Sens. Environ.* 113 (2009) S56–S66.  
1098 <https://doi.org/10.1016/J.RSE.2008.01.026>.
- 1099 [47] L. Dente, G. Satalino, F. Mattia, M. Rinaldi, Assimilation of leaf area index derived from  
1100 ASAR and MERIS data into CERES-Wheat model to map wheat yield, *Remote Sens.*  
1101 *Environ.* 112 (2008) 1395–1407. <https://doi.org/10.1016/j.rse.2007.05.023>.
- 1102 [48] D. Yu, Y. Zha, L. Shi, X. Jin, S. Hu, Q. Yang, Improvement of sugarcane yield estimation  
1103 by assimilating UAV-derived plant height observations, *Eur. J. Agron.* 121 (2020)  
1104 126159. <https://doi.org/10.1016/j.eja.2020.126159>.
- 1105 [49] J. Han, L. Shi, Q. Yang, Z. Chen, J. Yu, Y. Zha, Rice yield estimation using a CNN-  
1106 based image-driven data assimilation framework, *F. Crop. Res.* 288 (2022) 108693.  
1107 <https://doi.org/10.1016/j.fcr.2022.108693>.
- 1108 [50] D. Wallach, P.J. Thorburn, Estimating uncertainty in crop model predictions: Current  
1109 situation and future prospects, *Eur. J. Agron.* 88 (2017) A1–A7.  
1110 <https://doi.org/10.1016/j.eja.2017.06.001>.
- 1111 [51] D. Wallach, P. Thorburn, S. Asseng, A.J. Challinor, F. Ewert, J.W. Jones, R. Rötter, A.  
1112 Ruane, Estimating model prediction error: Should you treat predictions as fixed or  
1113 random?, *Environ. Model. Softw.* 84 (2016) 529–539.  
1114 <https://doi.org/10.1016/j.envsoft.2016.07.010>.
- 1115 [52] S. Hu, L. Shi, K. Huang, Y. Zha, X. Hu, H. Ye, Q. Yang, Improvement of sugarcane  
1116 crop simulation by SWAP-WOFOST model via data assimilation, *F. Crop. Res.* 232  
1117 (2019) 49–61. <https://doi.org/10.1016/j.fcr.2018.12.009>.
- 1118 [53] I.M. Fattori Junior, M. dos Santos Vianna, F.R. Marin, Assimilating leaf area index data  
1119 into a sugarcane process-based crop model for improving yield estimation, *Eur. J. Agron.*  
1120 136 (2022) 126501. <https://doi.org/10.1016/j.eja.2022.126501>.

- 1121 [54] A. Tewes, H. Hoffmann, G. Krauss, F. Schäfer, C. Kerkhoff, T. Gaiser, New Approaches  
1122 for the Assimilation of LAI Measurements into a Crop Model Ensemble to Improve  
1123 Wheat Biomass Estimations, *Agronomy*. 10 (2020) 446.  
1124 <https://doi.org/10.3390/agronomy10030446>.
- 1125 [55] G. Nearing, S. Yatheendradas, W. Crow, X. Zhan, J. Liu, F. Chen, The Efficiency of  
1126 Data Assimilation, *Water Resour. Res.* (2018). <https://doi.org/10.1029/2017WR020991>.
- 1127 [56] H. He, L. Lei, J.S. Whitaker, Z. Tan, Impacts of Assimilation Frequency on Ensemble  
1128 Kalman Filter Data Assimilation and Imbalances, *J. Adv. Model. Earth Syst.* 12 (2020).  
1129 <https://doi.org/10.1029/2020MS002187>.
- 1130 [57] M.P.G. de Oliveira, R.P. Amaro, H.B. Pescarini, L.H.A. Rodrigues, Tomato growth in  
1131 production-like setting, (2021). <https://doi.org/10.25824/redu/EP4NGO>.
- 1132 [58] M. Oliveira, R. Amaro, H. Pescarini, L.H. Rodrigues, Dataset of tomato plants growth  
1133 observations obtained from multiple sources in a production-like setting, *SciELO Prepr.*  
1134 (2023) 2023–2035. <https://doi.org/10.1590/SCIELOPREPRINTS.7667>.
- 1135 [59] B.H.E. Vanthoor, P.H.B. de Visser, C. Stanghellini, E.J. van Henten, A methodology for  
1136 model-based greenhouse design: Part 2, description and validation of a tomato yield  
1137 model, *Biosyst. Eng.* 110 (2011) 378–395.  
1138 <https://doi.org/10.1016/j.biosystemseng.2011.08.005>.
- 1139 [60] M. Oliveira, Leveraging high frequency data for improving crop growth estimates,  
1140 (2023). <https://doi.org/10.5281/zenodo.7632419>.
- 1141 [61] M.P.G. de Oliveira, Leveraging data assimilation and monitoring data for improvement  
1142 of crop growth estimates in protected environments, Universidade Estadual de  
1143 Campinas, 2022. <https://hdl.handle.net/20.500.12733/4792>.
- 1144 [62] D. Wallach, D. Makowski, J.W. Jones, F. Brun, Regression Analysis, Frequentist, in: D.  
1145 Wallach, D. Makowski, J.W. Jones, F. Brun (Eds.), *Work. with Dyn. Crop Model.*, Third

- 1146 Edit, Elsevier, 2019: pp. 161–205. [https://doi.org/10.1016/B978-0-12-811756-9.00005-](https://doi.org/10.1016/B978-0-12-811756-9.00005-8)  
1147 8.
- 1148 [63] N. Zhang, X. Zhou, M. Kang, B.-G. Hu, E. Heuvelink, L.F.M. Marcelis, Machine  
1149 learning versus crop growth models: an ally, not a rival, *AoB Plants*. 15 (2022) 1–7.  
1150 <https://doi.org/10.1093/aobpla/plac061>.
- 1151 [64] S.H. van Delden, M. SharathKumar, M. Butturini, L.J.A. Graamans, E. Heuvelink, M.  
1152 Kacira, E. Kaiser, R.S. Klamer, L. Klerkx, G. Kootstra, A. Loeber, R.E. Schouten, C.  
1153 Stanghellini, W. van Ieperen, J.C. Verdonk, S. Violet-Chabrand, E.J. Woltering, R. van  
1154 de Zedde, Y. Zhang, L.F.M. Marcelis, Current status and future challenges in  
1155 implementing and upscaling vertical farming systems, *Nat. Food*. 2 (2021) 944–956.  
1156 <https://doi.org/10.1038/s43016-021-00402-w>.
- 1157 [65] M.G.J. Kallenberg, B. Maestrini, R. van Bree, P. Ravensbergen, C. Pylianidis, F. van  
1158 Evert, I.N. Athanasiadis, Integrating processed-based models and machine learning for  
1159 crop yield prediction, *ArXiv*. (2023). <http://arxiv.org/abs/2307.13466>.
- 1160 [66] D. Wallach, S. Buis, D.-M. Seserman, T. Palosuo, P. Thorburn, H. Mielenz, E. Justes,  
1161 K.-C. Kersebaum, B. Dumont, M. Launay, S.J. Seidel, A calibration protocol for soil-  
1162 crop models, *BioRxiv*. (2023). <https://doi.org/10.1101/2023.10.26.564162>.
- 1163 [67] D. Wallach, T. Palosuo, P. Thorburn, H. Mielenz, S. Buis, Z. Hochman, E. Gourdain, F.  
1164 Andrianasolo, B. Dumont, R. Ferrise, T. Gaiser, C. Garcia, S. Gayler, M. Harrison, S.  
1165 Hiremath, H. Horan, G. Hoogenboom, P.E. Jansson, Q. Jing, E. Justes, K.C. Kersebaum,  
1166 M. Launay, E. Lewan, K. Liu, F. Mequanint, M. Moriondo, C. Nendel, G. Padovan, B.  
1167 Qian, N. Schütze, D.M. Seserman, V. Shelia, A. Souissi, X. Specka, A.K. Srivastava, G.  
1168 Trombi, T.K.D. Weber, L. Weihermüller, T. Wöhling, S.J. Seidel, Proposal and  
1169 extensive test of a calibration protocol for crop phenology models, *Agron. Sustain. Dev.*  
1170 43 (2023) 1–14. <https://doi.org/10.1007/s13593-023-00900-0>.

- 1171 [68] M. Lamboni, D. Makowski, S. Lehuger, B. Gabrielle, H. Monod, Multivariate global  
1172 sensitivity analysis for dynamic crop models, *F. Crop. Res.* 113 (2009) 312–320.  
1173 <https://doi.org/10.1016/j.fcr.2009.06.007>.
- 1174 [69] S.J.J. Seidel, T. Palosuo, P. Thorburn, D. Wallach, Towards improved calibration of crop  
1175 models – Where are we now and where should we go?, *Eur. J. Agron.* 94 (2018) 25–35.  
1176 <https://doi.org/10.1016/j.eja.2018.01.006>.
- 1177 [70] D. Wallach, T. Palosuo, P. Thorburn, Z. Hochman, E. Gourdain, F. Andrianasolo, S.  
1178 Asseng, B. Basso, S. Buis, N. Crout, C. Dibari, B. Dumont, R. Ferrise, T. Gaiser, C.  
1179 Garcia, S. Gayler, A. Ghahramani, S. Hiremath, S. Hoek, H. Horan, G. Hoogenboom,  
1180 M. Huang, M. Jabloun, P.-E. Jansson, Q. Jing, E. Justes, K.C. Kersebaum, A.  
1181 Klosterhalfen, M. Launay, E. Lewan, Q. Luo, B. Maestrini, H. Mielenz, M. Moriondo,  
1182 H. Nariman Zadeh, G. Padovan, J.E. Olesen, A. Poyda, E. Priesack, J.W.M. Pullens, B.  
1183 Qian, N. Schütze, V. Shelia, A. Souissi, X. Specka, A.K. Srivastava, T. Stella, T. Streck,  
1184 G. Trombi, E. Wallor, J. Wang, T.K.D. Weber, L. Weihermüller, A. de Wit, T. Wöhling,  
1185 L. Xiao, C. Zhao, Y. Zhu, S.J. Seidel, The chaos in calibrating crop models: Lessons  
1186 learned from a multi-model calibration exercise, *Environ. Model. Softw.* 145 (2021)  
1187 105206. <https://doi.org/10.1016/j.envsoft.2021.105206>.
- 1188
- 1189

1190 **Supplementary Material A**1191 **Table A1. Parameters values before and after calibration.**

Parameter	Calibrated value	Non-calibrated value (Original set)
alpha_F	0.92	0.8
beta	0.5	0.169
delta	0.07	0.038
DFmax	0.033	0.08
E	0.75	0.75
K	0.58	0.58
K_F	8	5
m	0.1	0.1
N_b	15.5	16
N_FF	19.6	22
N_max	0.57	0.5
p_1	2	2
Q10	1.4	1.4
Qe	0.09	0.08
rm	0.016	0.016
sl_N1	0.025	0.025
sl_N2	0.05	0.05
sl_R	0.0032	0.0032
T_crit	28.4	24.4
tau1	0.07428	0.07428
tau2	0.05848	0.05848
tmaxPg	35	35
tmin_fr_gr	8.5	8.5
TQe	23	23
TSlop	20.6	20.6
V	0.135	0.135
V_max	8	8

1192

This preprint was submitted under the following conditions:

- The authors declare that they are aware that they are solely responsible for the content of the preprint and that the deposit in SciELO Preprints does not mean any commitment on the part of SciELO, except its preservation and dissemination.
- The authors declare that the necessary Terms of Free and Informed Consent of participants or patients in the research were obtained and are described in the manuscript, when applicable.
- The authors declare that the preparation of the manuscript followed the ethical norms of scientific communication.
- The authors declare that the data, applications, and other content underlying the manuscript are referenced.
- The deposited manuscript is in PDF format.
- The authors declare that the research that originated the manuscript followed good ethical practices and that the necessary approvals from research ethics committees, when applicable, are described in the manuscript.
- The authors declare that once a manuscript is posted on the SciELO Preprints server, it can only be taken down on request to the SciELO Preprints server Editorial Secretariat, who will post a retraction notice in its place.
- The authors agree that the approved manuscript will be made available under a [Creative Commons CC-BY](#) license.
- The submitting author declares that the contributions of all authors and conflict of interest statement are included explicitly and in specific sections of the manuscript.
- The authors declare that the manuscript was not deposited and/or previously made available on another preprint server or published by a journal.
- If the manuscript is being reviewed or being prepared for publishing but not yet published by a journal, the authors declare that they have received authorization from the journal to make this deposit.
- The submitting author declares that all authors of the manuscript agree with the submission to SciELO Preprints.